AFCRL - 72-0232

UNCLASSIFIED

INVESTIGATION OF THE ELEMENT PATTERN IN CYLINDRICAL PHASED ARRAYS OF CIRCULAR WAVEGUIDES

GUIRINO BALZANO

RAYTHEON CO., MISSILE SYSTEMS DIVISION
BEDFORD LABORATORIES
HARTWELL RD., BEDFORD, MASSACHUSETTS 01730

CONTRACT NO. F19628-70-C-0226

PROJECT NO. 4600

TASK NO. 460010

WORK UNIT NO. 46001001

SCIENTIFIC REPORT NO. 3
MARCH 1972

CONTRACT MONITOR: ALLAN C. SCHELL
MICROWAVE PHYSICS LABORATORY

Prepared for
AIR FORCE CAMBRIDGE RESEARCH LABORATORIES
AIR FORCE SYSTEMS COMMAND
UNITED STATES AIR FORCE
BEDFORD, MASSACHUSETTS 01730

56

UNCLASSIFIED

Security Classification

DOCUMENT CONTROL DATA - R&D

(Security classification of title, body of abstract and indexing annotation must be entered when the overall report is classified)

1. ORIGINATING ACTIVITY (Corporate author)	2a. REPORT SECURITY CLASSIFICATION
Raytheon Company, Missile Systems Division Radar Laboratory, Bedford, Mass. 01730	UNCLASSIFIED
	2b. GROUP

3. REPORT TITLE

INVESTIGATION OF THE ELEMENT PATTERN IN CYLINDRICAL PHASED ARRAYS OF CIRCULAR WAVEGUIDES

4. DESCRIPTIVE NOTES (Type of report and inclusive dates)

Scientific Interim

5. AUTHOR(S) (Last name, first name, initial)

Quirino Balzano

6. REPORT DATE	7a. TOTAL NO. OF PAGES	7b. NO. OF REFS
March 1972	56	14

8a. CONTRACT OR GRANT NO.	9a. ORIGINATOR'S REPORT NUMBER(S)
F19628-70-C-0226	
b. PROJECT, Task, Work Unit Nos. 4600-10-01	BR-6959 Scientific Report No. 3
c. DoD Element 62702F	9b. OTHER REPORT NO(S) (Any other numbers that may be assigned this report)
d. DoD Subelement 674600	AFCRL-72-0232

10. AVAILABILITY/LIMITATION NOTICES

A-Approved for public release; distribution unlimited

11. SUPPLEMENTARY NOTES	12. SPONSORING MILITARY ACTIVITY
TECH, OTHER	Air Force Cambridge Research Labs (LZ) L. G. Hanscom Field, Bedford, Mass. 01730

13. ABSTRACT

The radiation from the elements in a cylindrical phased array is analyzed theoretically and experimentally. The theoretical investigation has developed a multimodal analysis method for cylindrical arrays. The method is similar to that for plane arrays, whereby, the field inside the element is represented as the superposition of a set of waveguide modes. The method allows the definition and the precise evaluation of the driving point admittance of the elements. A comparison between the driving point admittance in planar and cylindrical arrays is made and the conditions for the use of Wheeler simulators for cylindrical array element design are set.

The experimental investigation has produced a considerable amount of data about the radiative properties of elements in cylindrical arrays. The radiation pattern and the gain of the elements have been examined in detail along with the array edge effects. The comparison between experimental and computed data shows that the theoretical methods provide excellent approximation of the array element radiation properties.

DD FORM 1 JAN 64 1473

UNCLASSIFIED

Security Classification

14. KEY WORDS	LINK A		LINK B		LINK C	
	ROLE	WT	ROLE	WT	ROLE	WT
CONFORMAL ARRAYS						
CYLINDRICAL ARRAYS						
ELEMENT PATTERN						
ELEMENT MATCHING NETWORK						

INSTRUCTIONS

1. ORIGINATING ACTIVITY: Enter the name and address of the contractor, subcontractor, grantee, Department of Defense activity or other organization *(corporate author)* issuing the report.

2a. REPORT SECURITY CLASSIFICATION: Enter the overall security classification of the report. Indicate whether "Restricted Data" is included. Marking is to be in accordance with appropriate security regulations.

2b. GROUP: Automatic downgrading is specified in DoD Directive 5200.10 and Armed Forces Industrial Manual. Enter the group number. Also, when applicable, show that optional markings have been used for Group 3 and Group 4 as authorized.

3. REPORT TITLE: Enter the complete report title in all capital letters. Titles in all cases should be unclassified. If a meaningful title cannot be selected without classification, show title classification in all capitals in parenthesis immediately following the title.

4. DESCRIPTIVE NOTES: If appropriate, enter the type of report, e.g., interim, progress, summary, annual, or final. Give the inclusive dates when a specific reporting period is covered.

5. AUTHOR(S): Enter the name(s) of author(s) as shown on or in the report. Enter last name, first name, middle initial. If military, show rank and branch of service. The name of the principal author is an absolute minimum requirement.

6. REPORT DATE: Enter the date of the report as day, month, year; or month, year. If more than one date appears on the report, use date of publication.

7a. TOTAL NUMBER OF PAGES: The total page count should follow normal pagination procedures, i.e., enter the number of pages containing information.

7b. NUMBER OF REFERENCES: Enter the total number of references cited in the report.

8a. CONTRACT OR GRANT NUMBER: If appropriate, enter the applicable number of the contract or grant under which the report was written.

8b, 8c, & 8d. PROJECT NUMBER: Enter the appropriate military department identification, such as project number, subproject number, system numbers, task number, etc.

9a. ORIGINATOR'S REPORT NUMBER(S): Enter the official report number by which the document will be identified and controlled by the originating activity. This number must be unique to this report.

9b. OTHER REPORT NUMBER(S): If the report has been assigned any other report numbers *(either by the originator or by the sponsor)*, also enter this number(s).

10. AVAILABILITY/LIMITATION NOTICES: Enter any limitations on further dissemination of the report, other than those imposed by security classification, using standard statements such as:

(1) "Qualified requesters may obtain copies of this report from DDC."

(2) "Foreign announcement and dissemination of this report by DDC is not authorized."

(3) "U. S. Government agencies may obtain copies of this report directly from DDC. Other qualified DDC users shall request through _____."

(4) "U. S. military agencies may obtain copies of this report directly from DDC. Other qualified users shall request through _____."

(5) "All distribution of this report is controlled. Qualified DDC users shall request through _____."

If the report has been furnished to the Office of Technical Services, Department of Commerce, for sale to the public, indicate this fact and enter the price, if known.

11. SUPPLEMENTARY NOTES: Use for additional explanatory notes.

12. SPONSORING MILITARY ACTIVITY: Enter the name of the departmental project office or laboratory sponsoring *(paying for)* the research and development. Include address.

13. ABSTRACT: Enter an abstract giving a brief and factual summary of the document indicative of the report, even though it may also appear elsewhere in the body of the technical report. If additional space is required, a continuation sheet shall be attached.

It is highly desirable that the abstract of classified reports be unclassified. Each paragraph of the abstract shall end with an indication of the military security classification of the information in the paragraph, represented as *(TS)*, *(S)*, *(C)*, or *(U)*.

There is no limitation on the length of the abstract. However, the suggested length is from 150 to 225 words.

14. KEY WORDS: Key words are technically meaningful terms or short phrases that characterize a report and may be used as index entries for cataloging the report. Key words must be selected so that no security classification is required. Identifiers, such as equipment model designation, trade name, military project code name, geographic location, may be used as key words but will be followed by an indication of technical context. The assignment of links, rules, and weights is optional.

AFCRL - 72-0232

UNCLASSIFIED

INVESTIGATION OF THE ELEMENT PATTERN IN CYLINDRICAL PHASED ARRAYS OF CIRCULAR WAVEGUIDES

QUIRINO BALZANO

RAYTHEON CO., MISSILE SYSTEMS DIVISION
BEDFORD LABORATORIES
HARTWELL RD., BEDFORD, MASSACHUSETTS 01730

CONTRACT NO. F19628-70-C-0226

PROJECT NO. 4600

TASK NO. 460010

WORK UNIT NO. 46001001

SCIENTIFIC REPORT NO. 3
MARCH 1972

CONTRACT MONITOR: ALLAN C. SCHELL
MICROWAVE PHYSICS LABORATORY

Prepared for
AIR FORCE CAMBRIDGE RESEARCH LABORATORIES
AIR FORCE SYSTEMS COMMAND
UNITED STATES AIR FORCE
BEDFORD, MASSACHUSETTS 01730

ABSTRACT

The radiation from the elements in a cylindrical phased array is analyzed theoretically and experimentally. The theoretical investigation has developed a multimodal analysis method for cylindrical arrays. The method is similar to that for plane arrays, whereby the field inside the element is represented as the superposition of a set of waveguide modes. The method allows the definition and the precise evaluation of the driving point admittance of the elements. A comparison between the driving point admittance in planar and cylindrical arrays is made and the conditions for the use of Wheeler simulators for cylindrical array element design are set.

The experimental investigation has produced a considerable amount of data about the radiative properties of elements in cylindrical arrays. The radiation pattern and the gain of the elements have been examined in detail along with the array edge effects. The comparison between experimental and computed data shows that the theoretical methods provide excellent approximation of the array element radiation properties.

TABLE OF CONTENTS

LIST OF ILLUSTRATIONS

LIST OF ILLUSTRATIONS (Cont.)

1. INTRODUCTION

This report presents some recent advances in conformal array theory and practice. The theoretical results consist of a "multimode" extension of the "single mode" method of analysis for infinite periodic cylindrical arrays of waveguide elements previously developed [1]. The method is similar to the approach used in planar array theory [3-4-5]. For the eigenexcitations of the cylindrical structure [1], the electric and magnetic fields external to the array are represented as a superposition of cylindrical space harmonics (cylindrical waves matching the periodicity of the eigenexcitation). The fields inside the elements are represented as a set of waveguide modes. In the array repetitive cell the continuity of the electric and magnetic fields is approximately enforced by using Galerkin's method. By properly increasing the number of waveguide modes and of space harmonics used in the computation, the array radiation can be characterized with any desired precision. This fact has not only theoretical value, but presents some practical advantages since the driving point admittance (for a given eigenexcitation) of an element in the array can be predicted accurately and matching networks designed on the basis of computations.

The practical results consist of a procedure for array element design. In cylindrical array practice, as in the plane case, one of the biggest difficulties lies in the design of a network for matching the radiating element to free space. In this report it is shown in what conditions the Wheeler simulator can be used in cylindrical array element design, and a design procedure is developed which is analogous to what Knittel and Diamond [12] have proposed for plane arrays. The method indicates how to check the correctness of the design, although it does not give an optimized (in some sense) synthesis method for the matching network. A final group of results of practical interest is represented by the outputs of the tests performed on a cylindrical array of 284 elements. The tests were directed toward proving the validity of the theoretical predictions of array element pattern. The

tests consisted in monitoring the receive pattern of an excited element with all other array elements match terminated. The experimental results are in excellent agreement with the computations, confirming the soundness of the theoretical approaches previously developed [1-2].

The report is organized in the following way. In Section 2 the method of analysis for infinite periodic cylindrical arrays is briefly presented along with some computations showing the difference between "single" and "multi-mode" analysis. Section 3 is devoted to a suggested procedure for cylindrical array design. In Section 4 the array used in the experimental tests is shown. The experimental data are presented and compared with numerical results.

2. MULTIMODE ANALYSIS OF INFINITE PERIODIC CYLINDRICAL ARRAYS OF CIRCULAR APERTURES

2.1 Aperture Field Match

Multimode methods of analysis of the radiation from an infinite periodic array of waveguide slots have been already presented in the literature [6-7] for rectangular waveguides. In the following a multimode method for circular elements fed by waveguides of identical radius will be presented. The method is an extension of the eigenexcitation approach given in Reference 1.

The elements may be filled with dielectric. Only the two orthogonal TE_{11} modes circumferentially and axially polarized are assumed to be propagating in the feed guide. The vector mode functions for the TE_{11} mode polarized in the axial and circumferential direction will be noted by $\underline{e}_a(\underline{s})$ and $\underline{e}_c(\underline{s})$ respectively, $\underline{s}$ being a position vector. All other modes $\underline{e}_s(\underline{s})$ are ordered by increasing cut-off frequency. To simplify the treatment the element aperture tangential electric field distribution is assumed to be represented with good accuracy by a superposition of the TE_{11}'s and the first Ω modes [8]. Then, with the notations of Section 3 of Reference 1, for a given eigenexcitation $\underline{e}(\underline{u}_o)$ the tangential electric field of the reference element excited with axial polarization can be represented by

$$\underline{E}_t^-(\underline{s}) = \sqrt{\frac{2}{G_a}}\sqrt{\frac{h}{2\pi N}}\left\{[1+\Gamma_a(\underline{u}_o)]\,\underline{e}_a(\underline{s}) + \Gamma_{ac}(\underline{u}_o)\,\underline{e}_c(\underline{s}) + \sum_{s=1}^{\Omega}\Gamma_{as}(\underline{u}_o)\,\underline{e}_s(\underline{s})\right\} \qquad (2\text{-}1)$$

where $\Gamma_a(\underline{u}_o)$ is the reflection coefficient of the excited axial mode, and $\Gamma_{ac}(\underline{u}_o)$ and $\Gamma_{as}(\underline{u}_o)$ are cross coupling coefficients representing the passive excitation of the other modes.

The traverse electric field on the cylindrical surface can be represented by the following Floquet's double series [1]:

$$\underline{E}_t^+(\underline{s}) = \sum_{p=-\infty}^{+\infty} \sum_{q=-\infty}^{+\infty} \underline{A}(\underline{u}opq)\, e^{-j\underline{\lambda}_{opq}\underline{s}} \qquad (2\text{-}2)$$

The continuity of the tangential electric field is approximately enforced by applying a procedure entirely similar to the plane case [3]; one obtains the following expression for the space harmonics:

$$\frac{C}{2\pi}\,\underline{A}(\underline{u}_{opq}) = \sqrt{\frac{2}{G_a}}\sqrt{\frac{h}{2\pi N}}\left\{[1+\Gamma_a(\underline{u}_o)]\,\underline{\mathcal{E}}_a(\underline{u}_{opq}) + \Gamma_{ac}(\underline{u}_o)\,\underline{\mathcal{E}}_c(\underline{u}_{opq}) + \sum_{s=1}^{Q}\Gamma_{as}(\underline{u}_o)\,\underline{\mathcal{E}}_s(\underline{u}_{opq})\right\} \qquad (2\text{-}3)$$

where C is the area of the elementary cell and $\underline{\mathcal{E}}_a(\underline{u}_{opq})$, $\underline{\mathcal{E}}_c(\underline{u}_{opq})$ and $\underline{\mathcal{E}}_s(\underline{u}_{opq})$ are the Fourier transforms of the modes $\underline{e}_a(\underline{s})$, $\underline{e}_c(\underline{s})$ and $\underline{e}_s(\underline{s})$ whose explicit expressions are given in Appendix A.

The continuity of the magnetic field can be approximately enforced by an analogous procedure. With the notations of Section 3 of [1], the tangential magnetic field at the reference element aperture is given by:

$$\underline{H}_t^-(\underline{s}) = \hat{\rho}_o x \left\{[(1-\Gamma_a(\underline{u}_o))\,G_{ao} + (1+\Gamma_a(\underline{u}_o))jB_{ao}]\,\underline{e}_a(\underline{s}) - \Gamma_{ac}(\underline{u}_o)\,(G_{co}-jB_{co})\,\underline{e}_c(\underline{s}) - \sum_{s=1}^{Q}\Gamma_{as}(\underline{u}_o)Y_s\underline{e}_s(\underline{s})\right\}\sqrt{\frac{2}{G_a}}\sqrt{\frac{h}{2\pi N}} \qquad (2\text{-}4)$$

where the Y_s are the characteristic admittances of the modes $\underline{e}_s(\underline{s})$.

The external tangential magnetic field is given by the following Floquet's expansion

$$\underline{H}_t^+(s) = \sqrt{\frac{2}{G_a}}\sqrt{\frac{h}{2\pi^N}}\frac{1}{jk\eta}\sum_{p=-\infty}^{+\infty}\sum_{q=-\infty}^{+\infty} e^{-j\underline{u}_{opq}\cdot s}\Big\{[a(\underline{u}_{opq})A_\phi(\underline{u}_{opq})$$

$$+b(\underline{u}_{opq})A_z(\upsilon_{opq})]\hat{z} + [c(\underline{u}_{opq})\,A_\phi(\underline{u}_{opq}) + d(\underline{u}_{opq})\,A_z(\underline{u}_{opq})]\,\hat{\phi}\Big\} \quad (2\text{-}5)$$

where $A_\phi(\underline{u}_{opq})$ and $A_z(\underline{u}_{opq})$ are the components of $\underline{A}(\underline{u}_{opq})$; $a(\underline{u}_{opq})$, $b(\underline{u}_{opq})$, $c(\underline{u}_{opq})$ and $d(\underline{u}_{opq})$ are given in [1].

If the equality of the $\underline{H}_t^-(s)$ and $\underline{H}_t^+(s)$ is approximately enforced, the following set of equations is obtained (Appendix B):

$$G_{ao} - [L_{aa}(\underline{u}_o) - jB_{ao}] = \Gamma_a(\underline{u}_o)[L_{aa}(\underline{u}_o) + G_{ao} - jB_{ao}]$$

$$+ \Gamma_{ac}(\underline{u}_o)L_{ac}(\underline{u}_o) + \sum_{s=1}^{Q}\Gamma_{as}(\underline{u}_o)L_{as}(\underline{u}_o) \quad (2\text{-}6)$$

$$-L_{ca}(\underline{u}_o) = \Gamma_a(\underline{u}_o)\,L_{ca}(\underline{u}_o) + \Gamma_{ac}(\underline{u}_o)[L_{cc}(\underline{u}_o) + G_{co} - jB_{co}]$$

$$+ \sum_{s=1}^{Q}\Gamma_{as}(\underline{u}_o)\,L_{cs}(\underline{u}_o) \quad (2\text{-}7)$$

$$-L_{ka}(\underline{u}_o) = \Gamma_a(\underline{u}_o)\,L_{ka}(\underline{u}_o) + \Gamma_{ac}(\underline{u}_o)\,L_{kc}(\underline{u}_o)$$

$$+ \sum_{s=1}^{Q}\Gamma_{as}(\underline{u}_o)[L_{ks}(\underline{u}_o) + \delta_{ks}Y_s] \quad (2\text{-}8)$$

where δ_{ks} is Kronecker's delta and $L_{rt}(\underline{u}_o)$ are rather complicated functions, whose explicit expressions are given in Appendix B. The physical interpretation of the $L_{rt}(\underline{u}_o)$ is that of self ($r = t$) and mutual ($r \neq t$) admittance of the

modes for a given eigenexcitation. Once the system of Equations (Equations (2-6) through (2-8)) is solved, the tangential electric field distribution at the element apertures is determined and their pattern can be straightforwardly obtained by applying the methods described in [1]. It is worth noticing that the system of equations (Equations (2-6) through (2-8)) provides the reflection coefficient $\Gamma_a(\underline{u}_o)$ of the actively excited mode and the amplitude of the voltages of the other modes excited at the aperture, if G_{ao} and B_{ao} (parameters of the matching network) are known. On the other hand if the system of equations (Equations (2-6) through (2-8)) is solved for $Y_{ao} = G_{ao} + jB_{ao}$ by imposing the condition $\Gamma_a(\underline{u}_o) = 0$, the resulting value of Y_{ao} represents the driving point admittance of the actively excited mode for a given eigenexcitation.

So far only the axial mode has been actively excited. If the circumferential TE_{11} is actively excited (with the same eigenexcitation in the array) a perfectly similar treatment can be done, obtaining the equations for the reflection coefficient $\Gamma_c(u_o)$ and the voltages of the other modes passively excited at the aperture. The new system of equations is obtained by permuting the subscripts a and c in Equations (2-6) through (2-8). The general case is obtained by superposition. Some numerical results obtained by applying multimodal analysis to a particular cylindrical array are shown in the next section.

2.2 Numerical Results

A few illustrative examples of the results given by the multimode analysis will be presented here. They are intended to show the difference between "one mode" and "multimode" analysis. For this purpose only results of computations relative to an array previously analyzed [1] will be presented. The cylinder radius is approximately 11 wavelengths and the element spacing is shown in Figure 2-1. The element aperture radius is 0.22λ and the element waveguides are filled by a dielectric with $\epsilon_r = 2.5$. In these conditions only the TE_{11} mode can propagate in the waveguides, all other modes being below cut-off.

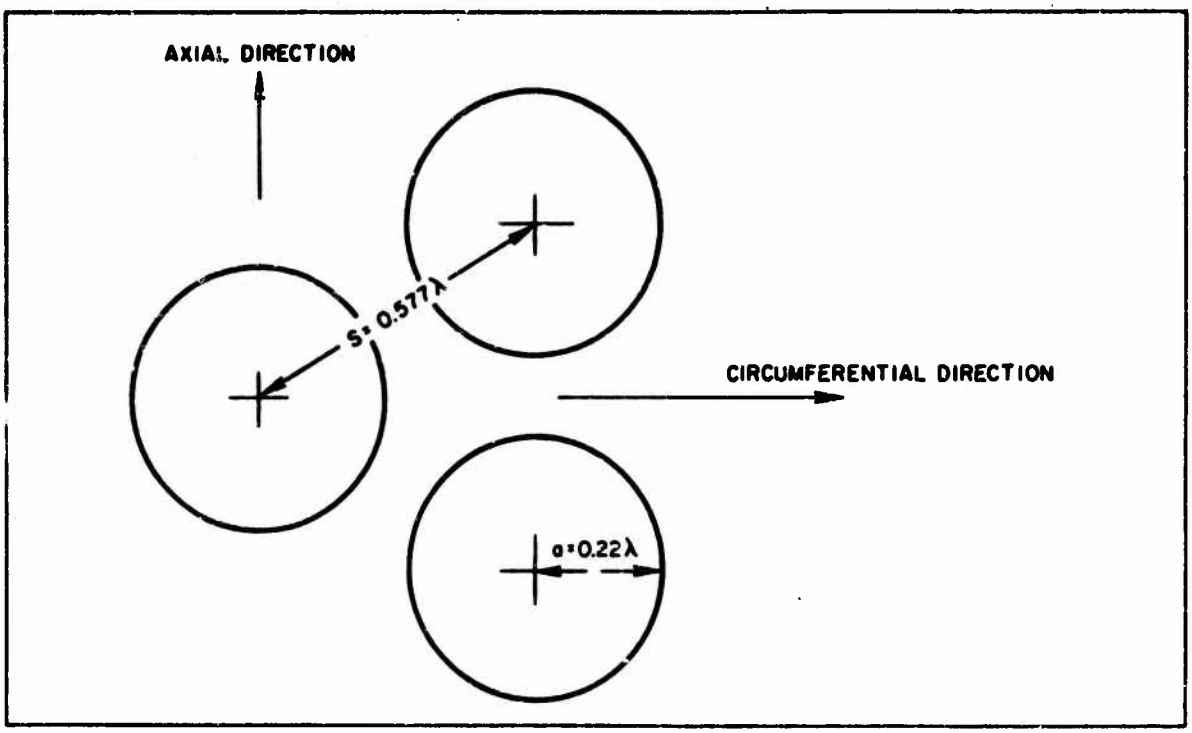

Figure 2-1 - Array Lattice

While performing numerical analysis, particular attention was devoted to the question of relative convergence [9] and no such condition was found for this special case. A relative convergence type of solution for cylindrical arrays is expected to exist only for the same kind of elements that give relative convergence in planar arrays [9]. Although no numerical research has been performed to prove it, this statement is thought to be basically correct since the relative convergence phenomenon seems to be related to the algebraic method of solution (i.e., Galerkin's or similar methods) rather than to the nature of space harmonics (planar or cylindrical) of the external fields. A set of element patterns for equiphase match [1] is shown in Figures 2-2 and 2-3 for circumferential and axial polarization respectively. On the same figure the "one mode" element pattern previously computed [1] is shown for reference.

No substantial variation is present in the element patterns for single mode or multimode analysis. The results show that as in the plane array case [4], the one mode approximation is indeed satisfactory unless second or third mode resonances are present [3].

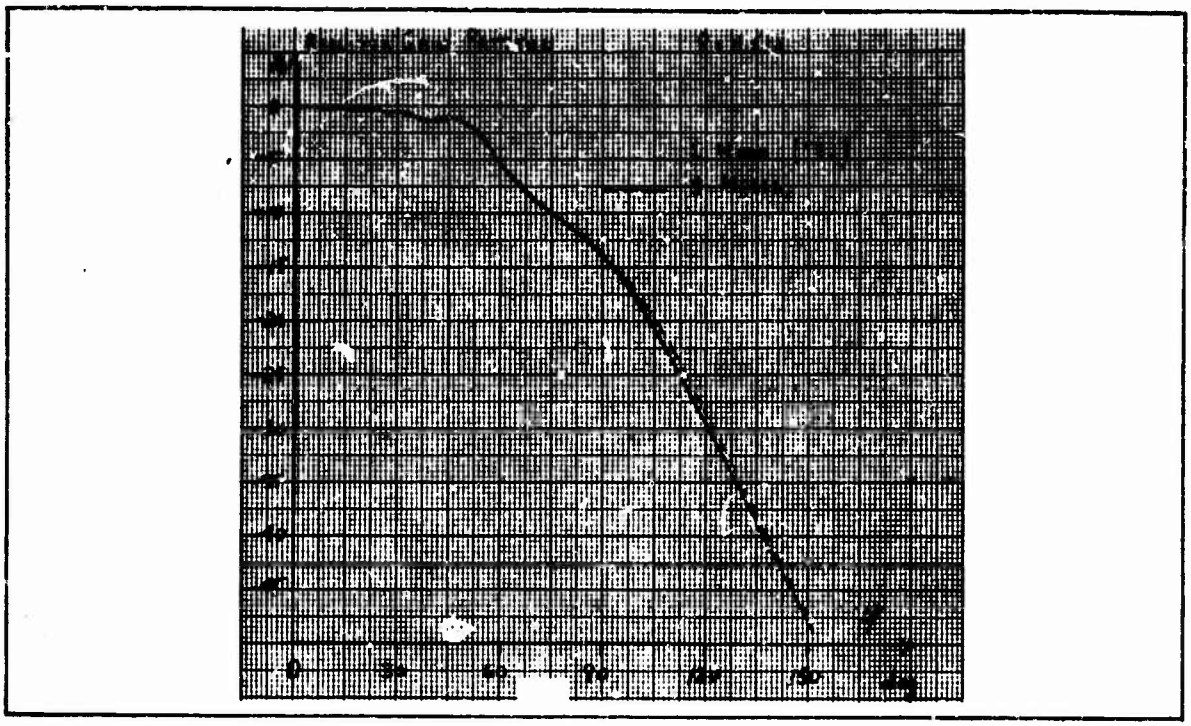

Figure 2-2 - Circumferential Polarization - Circumferential Cut Equiphase Match

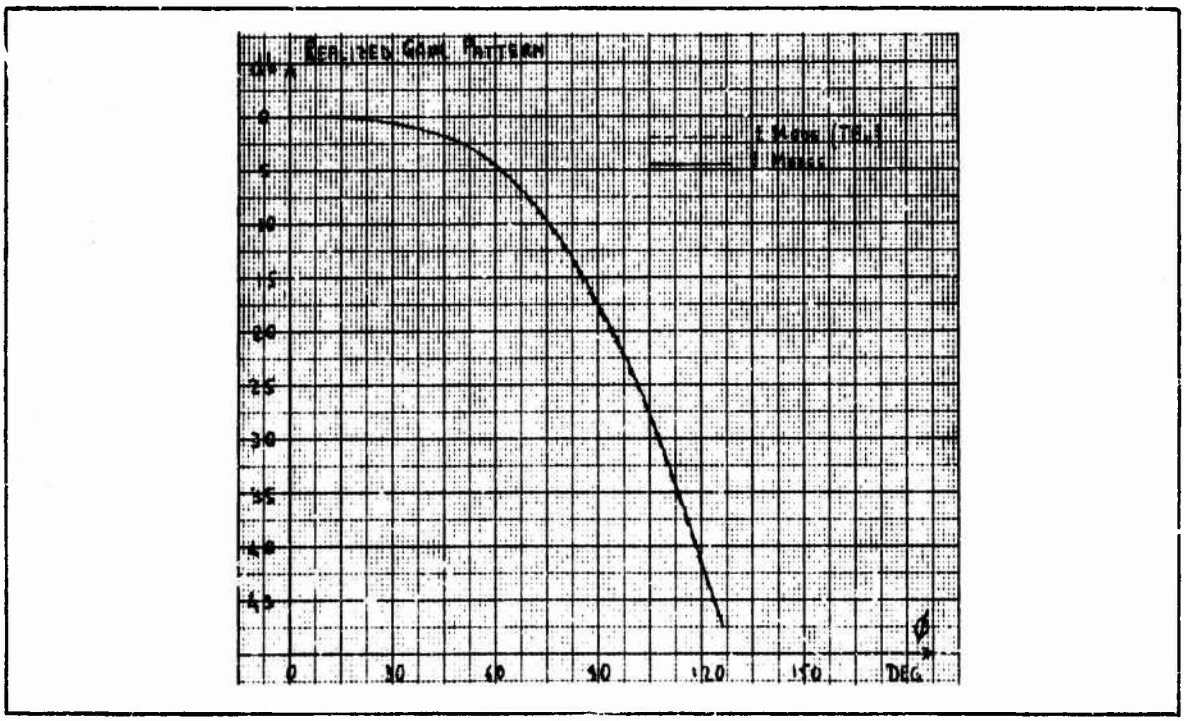

Figure 2-3 - Axial Polarization - Circumferential Cut - Equiphase Match

Figures 2-4 and 2-5 show the array element pattern in the circumferential plane for circumferential and axial polarization respectively. Both polarization ports are matched for the eigenexcitation [1] ($i/R = 2\pi/\lambda \sin 80°$, $w_o = 0$). In this case too no appreciable variation is detected in the results for one mode and multimode analysis. Similar behavior is shown by the patterns in the axial plane (Figures 2-6 and 2-7).

More substantial variation with the number of waveguide modes used in the computations is presented by the element driving point admittance for a given eigenexcitation. Figures 2-8 and 2-9 show the driving point admittance of the elements versus number of waveguide modes for the eigenexcitations $e(i/R = 2\pi/\lambda \sin 80°, w_o = 0)$ and $e(i/R = 0, w_o = 2\pi/\lambda \sin 80°)$ respectively. The absolute convergence of the driving point admittance versus number of waveguide modes (400 space harmonics have been consistently used in the computations) is clearly shown by Figures 2-8 and 2-9, since the computed values tend to a definite limit as the number of modes is increased. As can be seen, the one mode analysis would give admittance values considerably in error.

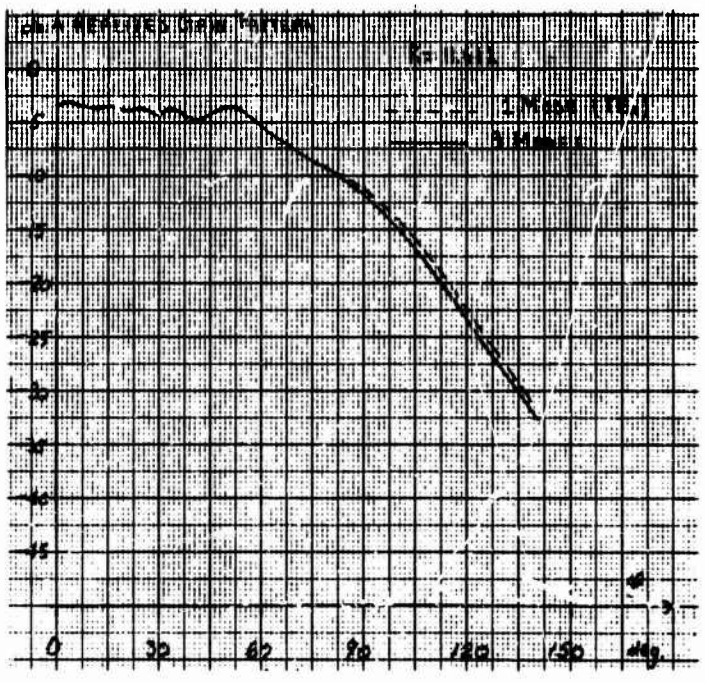

Figure 2-4 - Circumferential Polarization - Circumferential Cut - Match for $e(i/R = 2\pi/\lambda \sin 80°, w_o = 0)$

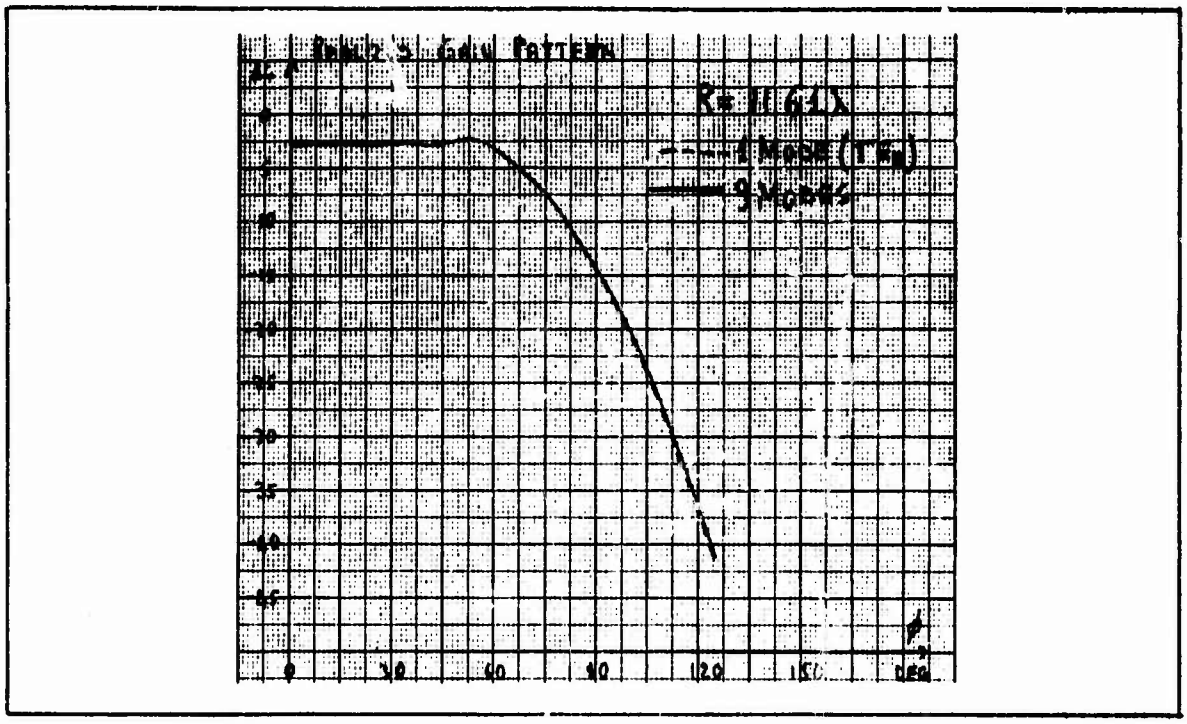

Figure 2-5 - Axial Polarization - Circumferential - Cut Match for $e(i/R = 2\pi/\lambda \sin 80°, w_o = 0)$

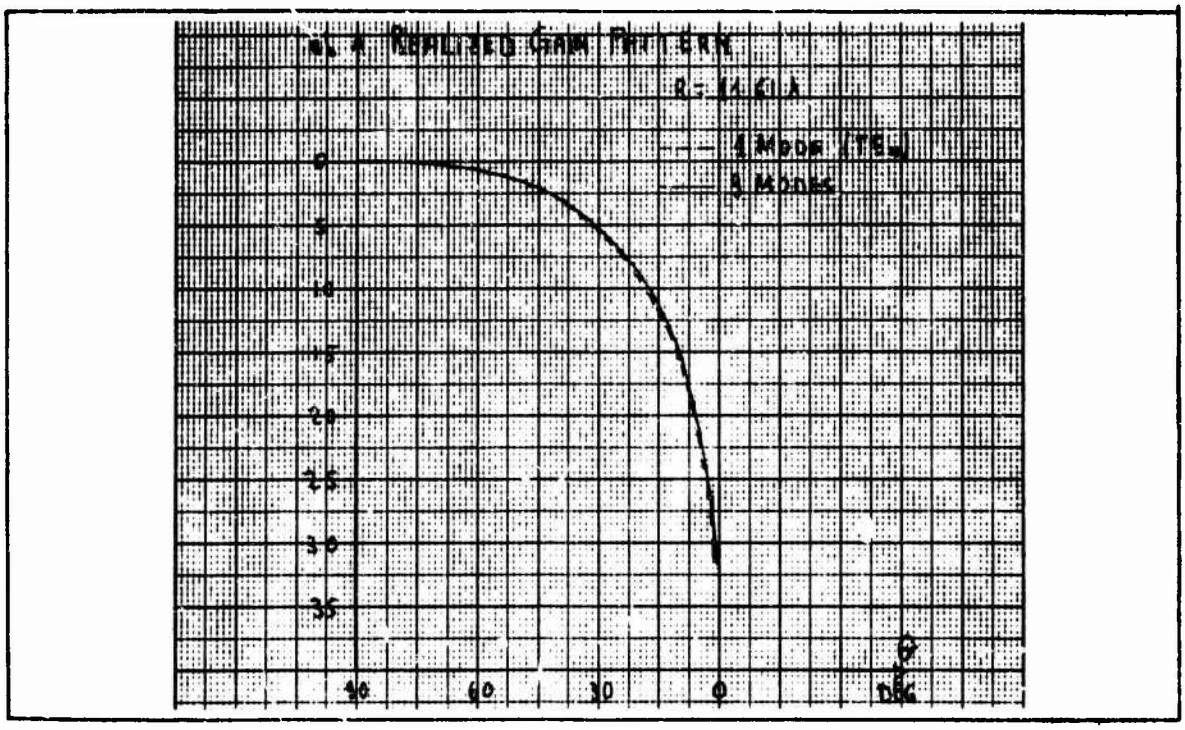

Figure 2-6 - Circumferential Polarization - Axial Cut - Equiphase Match

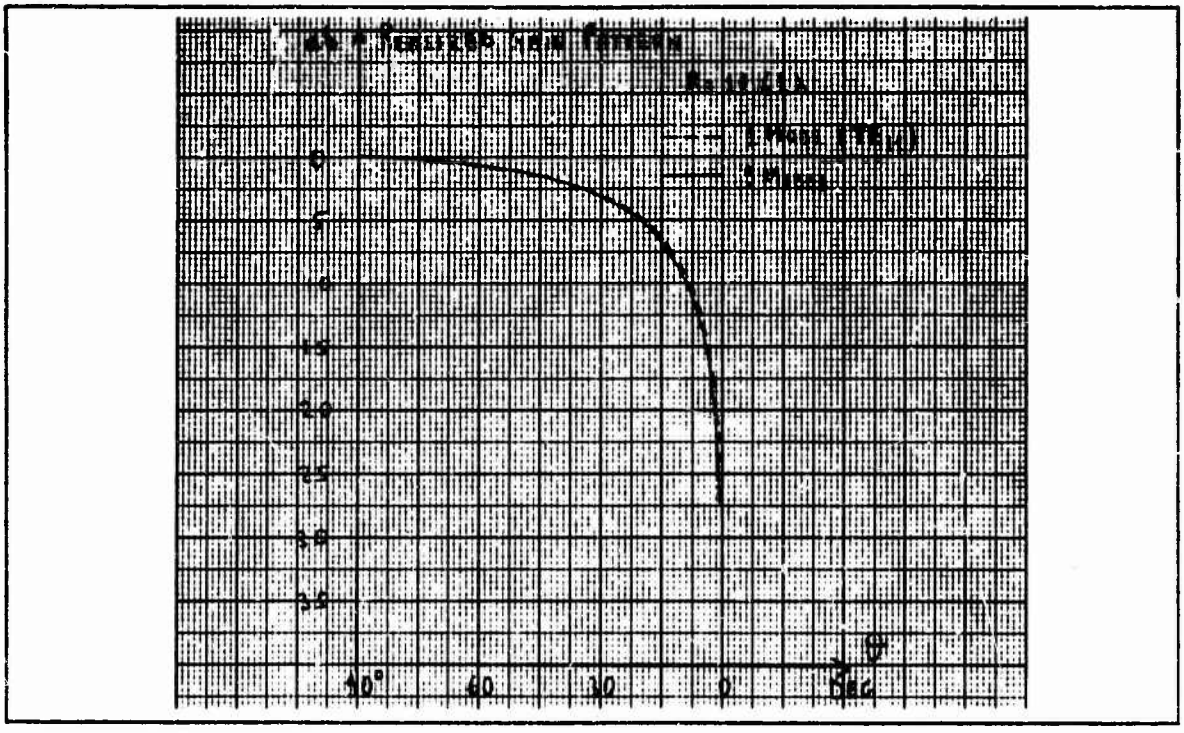

Figure 2-7 - Axial Polarization - Axial Cut - Equiphase Match

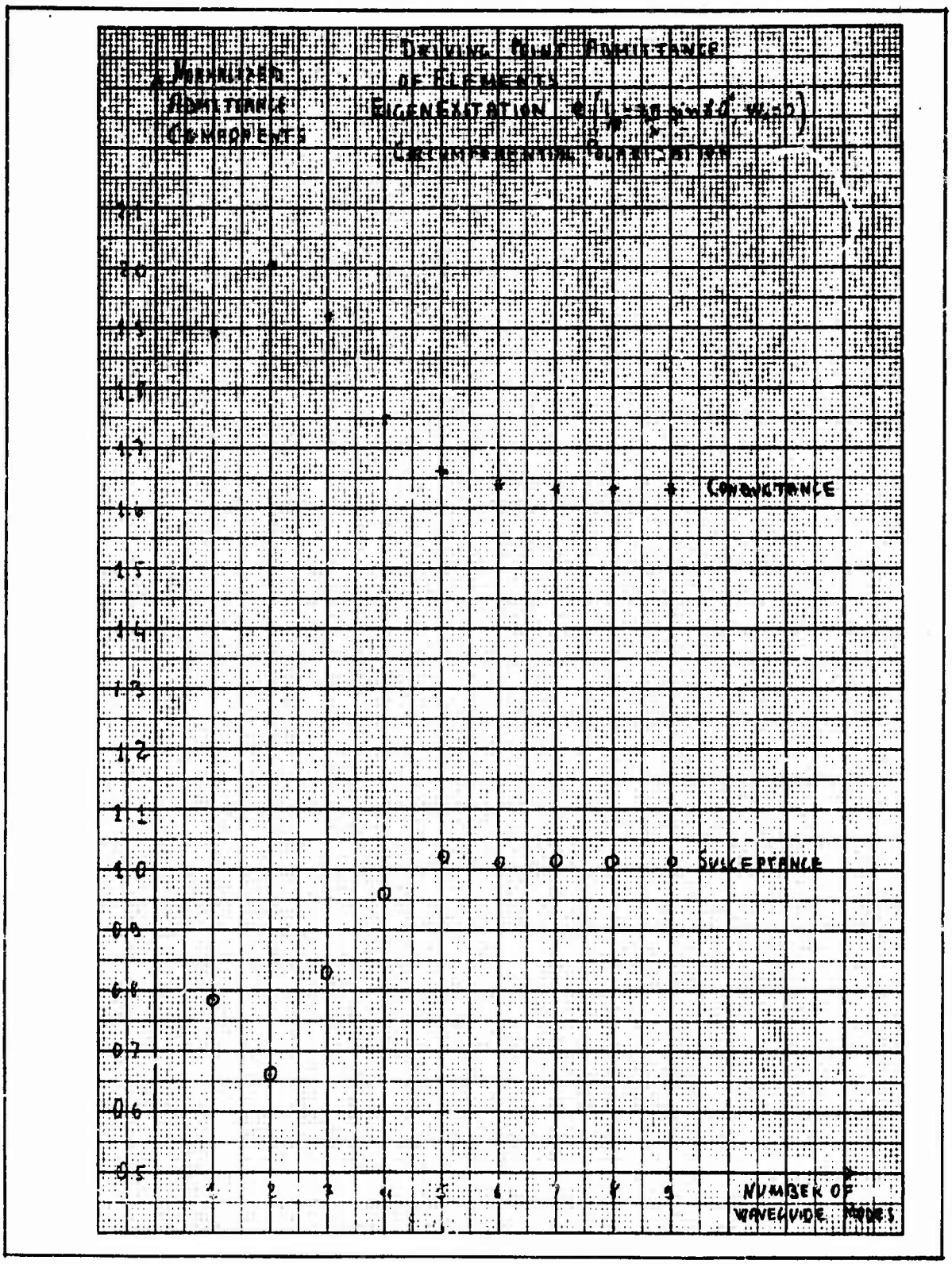

Figure 2-8 - Driving Point Admittance of Elements - Eigenexcitation ($e^{(i/R} = 2\pi/\lambda \sin 30°$, $w_o = 0$)

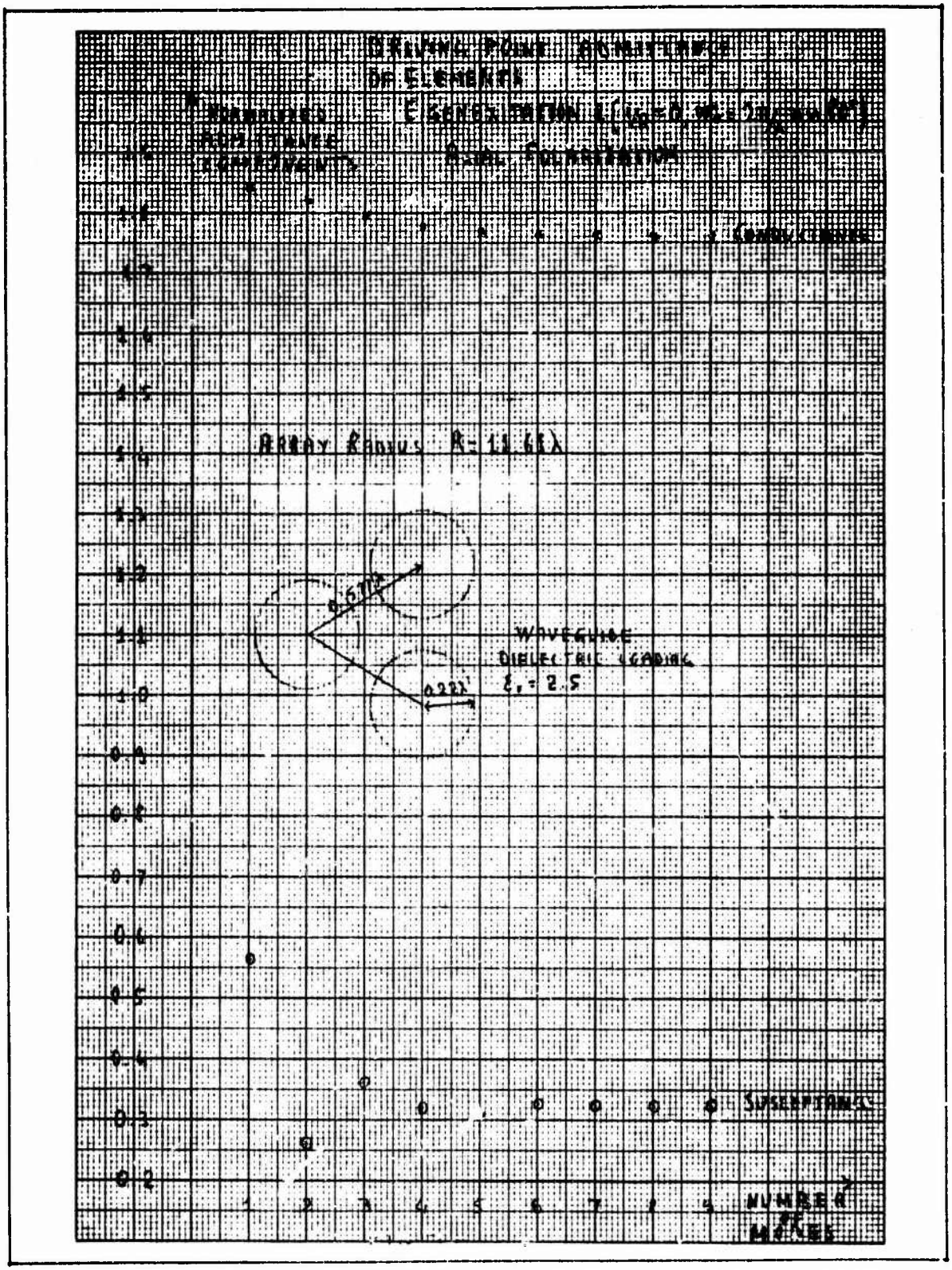

Figure 2-9 - Driving Point Admittance of Elements - Eigenexcitation $e(i/R = 0, w_o = 2\pi/\lambda \sin 80°)$

3. A PROCEDURE FOR THE DESIGN OF WAVEGUIDE ELEMENTS FOR A CONFORMAL PHASED ARRAY ON A CYLINDER

3.1 General Considerations

In cylindrical array design, as in plane array practice, one of the most difficult steps consists in the design of a network matching the radiating element to free space to reduce the reflection at the interface. Basically two approaches have been introduced for the design of plane array elements [10-11-12]:

1) Methods which rely on computed values of the element reflection coefficient to synthetize a matching network and on Wheeler simulators to confirm the correctness of the design
2) Small array techniques [10]. These are available, but are not recommended except in a few special cases.

It is worth noticing that these approaches only suggest ways of checking the design of a matching network and do not represent true network synthesis methods.

Of the two approaches mentioned previously only the small array techniques can be correctly applied to cylindrical arrays, since these antennas lack the symmetries required by the Wheeler simulators. Small array techniques, however, have a serious drawback, since in order to make a measurement of power reflected in the element, the array feed must be built, making the approach expensive. On the other hand, if measurements are performed with the small array in receive, so that no feed is required, the results are not very precise, since only the element patterns can be monitored, and these depend on the square of the reflection coefficient. Thus, one could be somewhat off in the desired matching condition of the elements and still monitor a good pattern.

From these considereations it seems that, for lack of a device like a Wheeler simulator, conformal array element design is bound to be either expensive or imprecise. Multimodal analysis and the concept of eigenexcitation help in alleviating this situation.

3.2 Comparison of Admittance Values in Cylindrical and Plane Arrays

In Section 2 it was shown that multimode analysis makes possible the computation of the array element driving point admittance for a given eigenexcitation. An eigenexcitation (or characteristic excitation) is characterized by the property of having the same transverse electric field distribution at the elements except for a progressive phase term. In an infinite cylindrical array an eigenexcitation gives rise to a cylindrical space harmonic matching the periodicity of the excitation, just as in planar arrays a linear phase front (eigenexcitation) produces a plane wave (plane space harmonic). The eigenexcitations bring out the similarity between cylindrical and planar arrays. There is, however, a substantial difference. When a plane array is phased to radiate in a certain direction all the elements are steered away from their normals by the same amount so that essentially one space harmonic is excited (except for edge effects) and a driving point admittance can be defined. When a cylindrical array is forced to radiate a plane wave in a given direction, not only one, but an infinite number of cylindrical space harmonics are excited, since the elements in general are steered in different directions from their normals. The same would happen if one tried to radiate a cylindrical wave from a planar array. Since an infinite number of space harmonics are excited, the array excitation must be given by the superposition of an infinite number of eigenexcitations, and a driving point admittance of the elements cannot be rigorously defined. However, it has been shown [1] that a particular set of space harmonics is strongly excited, namely the set with wavenumbers $(i/R, w_o)$ close to the direction cosines of the desired plane wave. Consequently to radiate this plane wave efficiently, the array elements must be matched to the admittance of the eigenexcitation $(i/R, w_o)$ and in this sense a driving point admittance can be defined. If all the elements are matched for the admittance of the eigenexcitation $(i/R, w_o)$, the array is not perfectly matched in an absolute sense, but is matched in the best possible way if the same network is used in each element. Of course, better matching conditions and higher array gain can be achieved in a given direction if different matching networks are used in the various elements. This solution, however, is not attractive in practive, especially for cylindrical arrays with a large number of elements.

Having defined what is meant by driving point admittance in a cylindrical array excited tc radiate a plane wave, let us compare cylindrical and planar values. Table 2-1 shows the computed admittance for a plane and a cylindrical array. The cylindrical array has a radius of 11.61λ and the spacing of Figure 2-1. The computations have been performed using a great number of waveguide modes (15) and space harmonics (400) so they are very precise for all practical purposes. As can be seen in the circumferential plane the circumferential polarization gives a substantial difference between plane and cylindrical array, but in the axial plane for axial polarization the variation is slight.

Table 2-2 gives the computed values of the element driving point admittance in the circumferential plane for axial polarization. The discrepancy between this and the corresponding planar case is very small for eigenexcitations with wave number up to $i/R = 2\pi/\lambda \sin 60°$. On the other hand substantial differences are shown by the admittance values of plane and cylindrical arrays in the axial plane for circumferential polarization (Table 2-3). This behavior of the element driving point admittance can be simply explained. It is well known [13] that element mutual coupling, the determining factor of the driving point admittance, occurs mainly in directions close to the E-plane of the elements, while there is relatively little coupling along the H-plane direction. For this reason axially polarized elements on a cylinder are coupled in a manner similar to that for the elements of a plane array (for a cylinder radius of about 10λ or more). Only when phasing conditions are such as to strongly excite H-plane coupling (eigenexcitations with wave number i/R close to $2\pi/\lambda$), does the presence of the curvature affect the element driving point admittance, causing a difference between cylindrical and planar case. The opposite is true for circumferentially polarized elements. Since their coupling occurs basically along the direction of the cylinder curvature, a substantial departure from the plane case can be expected. Only when excited so as to radiate at extreme angles in the axial plane do the circumferentially polarized elements of a cylindrical array approach the planar array coupling conditions. However, as the cylinder radius is increased, one can expect that the circumferentially polarized elements will approach planar mutual coupling conditions.

TABLE 3-1

NORMALIZED DRIVING POINT ADMITTANCE VALUES

Axial Polarization - Axial Plane			
Plane Array		Cylindrical Array (R = 11.61)	
Broadside	0.5173 - j0.6818	$e(i/R = 0, w_o = 0)$	0.5174 - j0.6685
80 deg from Broadside	1.7014 + j0.3299	$e(i/R = 0, w_o = 2\pi/\lambda \sin 80°)$	1.7571 + j0.3289
Circumferential Polarization - Circumferential Plane			
Broadside	0.5173 - j0.6743	$e(i/R = 0, w_o = 0)$	0.5173 - j0.4410
80 deg from Broadside	2.1306 + j1.2389	$e(i/R = 2\pi/\lambda \sin 80°, w_o = 0)$	1.6435 + j1.0133

TABLE 3-2

NORMALIZED DRIVING POINT ADMITTANCE VALUES

Axial Polarization - Circumferential Plane			
Plane Array		Cylindrical Array (R = 11.61)	
40 deg from Broadside	0.3498 - j0.5410	$e(i/R = 2\pi/\lambda \sin 40°, w_o = 0)$	0.3431 - j0.5067
60 deg from Broadside	0.2073 - j0.4198	$e(i/R = 2\pi/\lambda \sin 60°, w_o = 0)$	0.2213 - j0.4279
80 deg from Broadside	0.0670 - j0.3165	$e(i/R = 2\pi/\lambda \sin 80°, w_o = 0)$	0.1452 - j0.2913

TABLE 3-3

NORMALIZED DRIVING POINT ADMITTANCE VALUES

Circumferential Polarization - Axial Plane			
Plane Array		Cylindrical Array (R = 11.61)	
40 deg from Broadside	0.3507 - j0.4986	$e(i/R = 0, w_o = 2\pi/\lambda \sin 40°)$	0.3862 - j0.3363
60 deg from Broadside	0.2071 - j0.3071	$e(i/R = 0, w_o = 2\pi/\lambda \sin 60°)$	0.2963 - j0.2141
80 deg from Broadside	0.0674 - j0.1574	$e(i/R = 0, w_o = 2\pi/\lambda \sin 80°)$	0.0822 - j0.1190

Let us suppose now that a Wheeler simulator is used to design an axially polarized element of a cylindrical array with radius of 10λ or more. The element matching network would be matched at the planar array admittance value and an error would be present. This error however is going to be far smaller than when using a small array in receive, which constitutes a design tool comparable in cost to a Wheeler simulator.

3.3 A Design Method Foe Cylindrical Array Elements

From the preceding considerations it is clear that the design of axially polarized elements on cylindrical arrays with radius greater than 10λ can follow the guidelines used in planar array practice. A procedure for cylindrical array element design, similar to the one proposed by Diamond and Knittel [12] for plane arrays, is suggested here and is based on the use of computations and Wheeler simulators. The procedure consists of four steps:

1) Select the element geometry and the matched eigenexcitation so as to achieve the required coverage
2) Compute the driving point admittance of the array (in the sense specified at 3.2 versus scan conditions and frequency)
3) Synthetize a matching (to the selected eigenexcitation) network on the basis of previous computations
4) Confirm the network design by the means of a Wheeler simulator in the axial or circumferential plane

As pointed out before, the procedure can be applied only to cylinders with radius bigger than 10λ and axially polarized elements. If the cylinder radius is increased, the preceding method can become of general application. A bound to the error in each case can be evaluated by performing an accurate computation of the driving point admittance of planar and cylindrical arrays.

4. EXPERIMENTAL INVESTIGATION

4.1 Experimental Program

An experimental program has been conducted to check the validity of the theoretical methods for the determination of the array element pattern [1-2]. In particular, the program included experimental tests to check the modification of the realized gain pattern due to the matching network (pattern shaping network) introduced [1] to increase the coverage of the array. The tests consisted in monitoring the gain and the receive patterns in the axial and circumferential plane of an excited radiator with all other elements match terminated. The excited element was moved within the array to record edge effects.

The tests were performed on the cylindrical array shown in Figure 4-1. The cylindrical structure has a radius of 16.5 in., corresponding to 11.61λ at 8.3 GHz, the frequency of operation of the array. The element lattice is the one shown in Figure 2-1. The element spacing is 0.81 in. corresponding to 0.577λ at 8.3 GHz. Conventionally the array rows are in the circumferential direction, the columns in the axial. The angular extent of the array is about 50 deg. The array shape is approximately a square with 12-in. sides. There are 27 rows and 21 columns. The height of the cylinder is about 20 in. The edges have been extended and rounded with a structure (not shown in Figure 4-1) to decrease the ground plane edge effects. There are 284 elements in the array. The elements are circular waveguides with 0.32 in. radius, corresponding to 0.22λ at 8.3 GHz. At this frequency only the TE_{11} mode is propagating and all others are below cut-off. The waveguides are match terminated. Only one element is excited and its waveguide terminates in a transition to rectangular waveguide. The transition was designed for this application and was matched very carefully at 8.3 GHz.

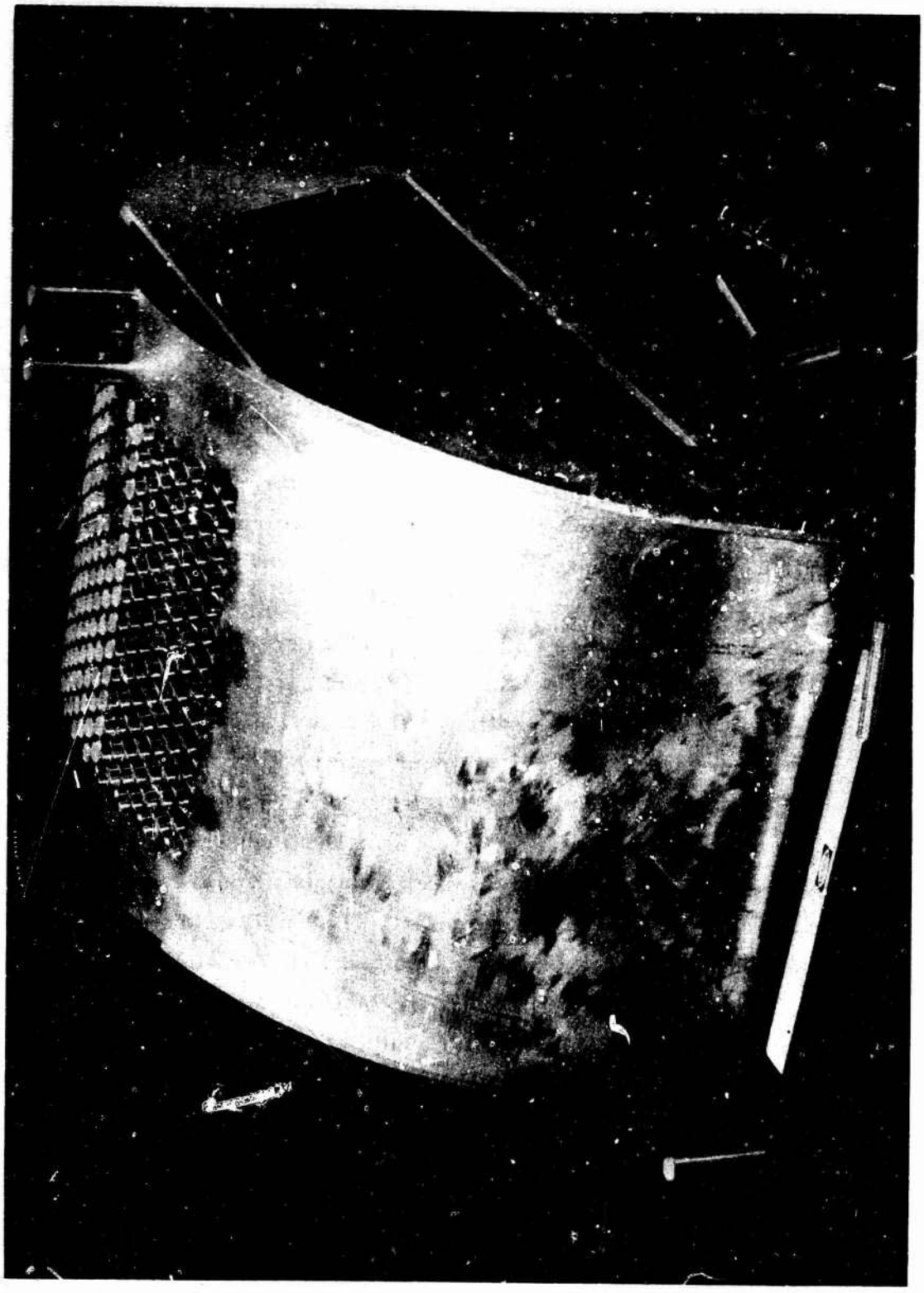

71 62694

Figure 4-1 - Conformal Array

Tests were performed for four different element shaping networks in the waveguides. With reference to Section 1, the element apertures were matched for the following three different eigenexcitations:

1) e(i/R = 0, w_o = 0), equiphase excitation [1], corresponding to broadside match in planar arrays. Both circumferential and axial polarization matching networks have been built.
2) e(i/R = $2\pi/\lambda$ sin 80°, w_o = 0), corresponding to matching at 80 deg from broadside in the circumferential direction for a plane array. Only the circumferential polarization has been matched for this eigenexcitation.
3) e(i/R = 0, w_o = $2\pi/\lambda$ sin 80°), corresponding to a match at 80 deg from broadside in the axial direction for a planar array. Only the axial polarization has been matched in this condition.

An element with its four matching networks is shown in Figure 4-2. The networks were designed on the basis of the numerical computations of the driving point admittance presented in Section 1. The desired matching

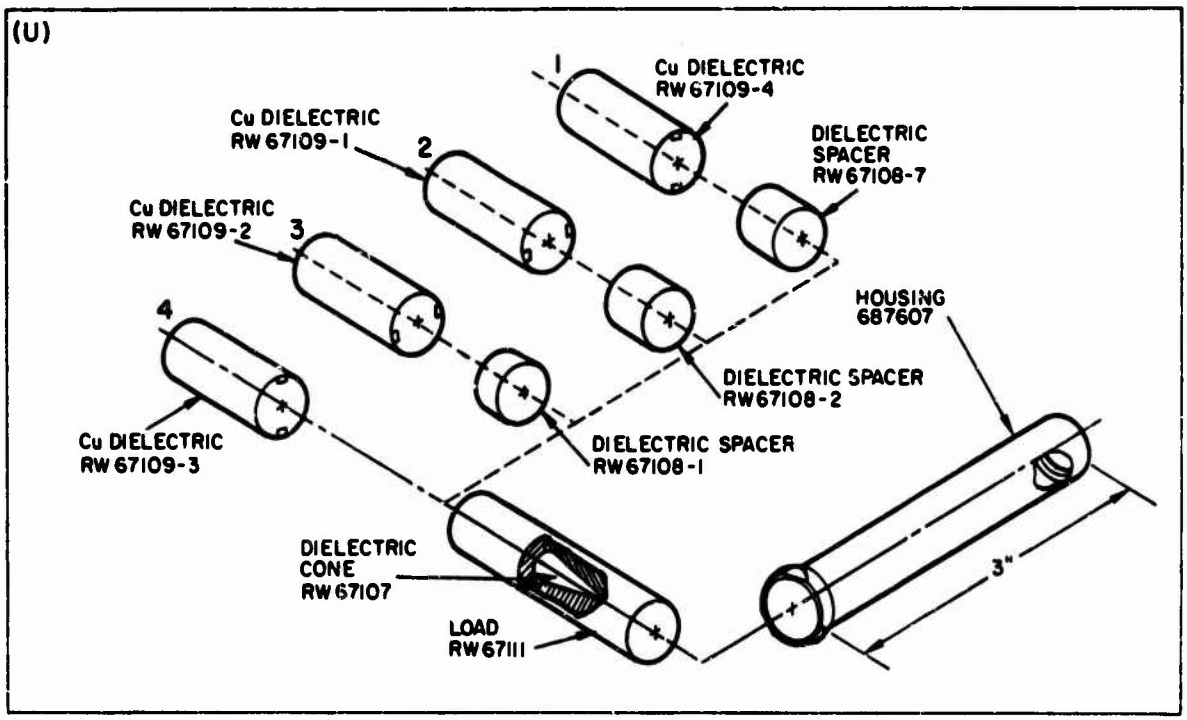

Figure 4-2 - Conformal Array Element

conditions for the elements are obtained by plating a copper coating and two copper tabs of a certain penetration on the dielectric filling the waveguide at a suitable distance from the aperture. The networks match only one polarization (the other one is simply terminated) since the two polarizations are completely decoupled for scanning in the axial and the circumferential plane. With reference to Figure 4-2, the networks 1 and 2 match axial and circumferential polarization respectively for the eigenexcitation e(i/R = 0, w_o = 0), network 3 matches the circumferential polarization for e(i/R = $2\pi/\lambda$ sin 80°, w_o = 0) and network 4 the axial polarization for e(i/R = 0, $w_o = 2\pi/\lambda$ sin 80°). The patterns presented in the following paragraph were recorded at the antenna range of the Bedford Facilities of Raytheon Company.

4.2 Experimental Results

A large amount of experimental data has been collected. The element patterns relative to the axial polarization in the axial plane show interesting effects due to the finite size of both array and ground plane. A set of these experimental data will be presented first.

Figure 4-3 shows the recorded pattern in the axial plane of an element at the center of the array. The elements are axially polarized and are matched for the eigenexcitation e(i/R = 0, w_o = 0) (equiphase match). Superimposed on the recorded pattern are the computations using the infinite array model, plotted with a broken line. The solid line represents the pattern computed with the finite array model [2]. This model represents the antenna as a finite array over an infinite conducting cylinder.

There are two edge effects worthwhile noticing in Figure 4-3. The first is due to the finite dimension of the ground plane and causes the experimental pattern to depart from the data computed with the infinite ground plane model in the last 18 deg before endfire. The other is due to the array finite dimensions and forces the radiation of the element in the region 50 - 70 deg from the element normal below the level predicted for the infinite array model of as much as 2 dB. The result shows how inaccurate the infinite array model is in predicting the gain versus scan for a 30 dB array. Interestingly enough, the infinite model is too optimistic in predicting the element gain in the region 50 - 70 deg from the radiator normal.

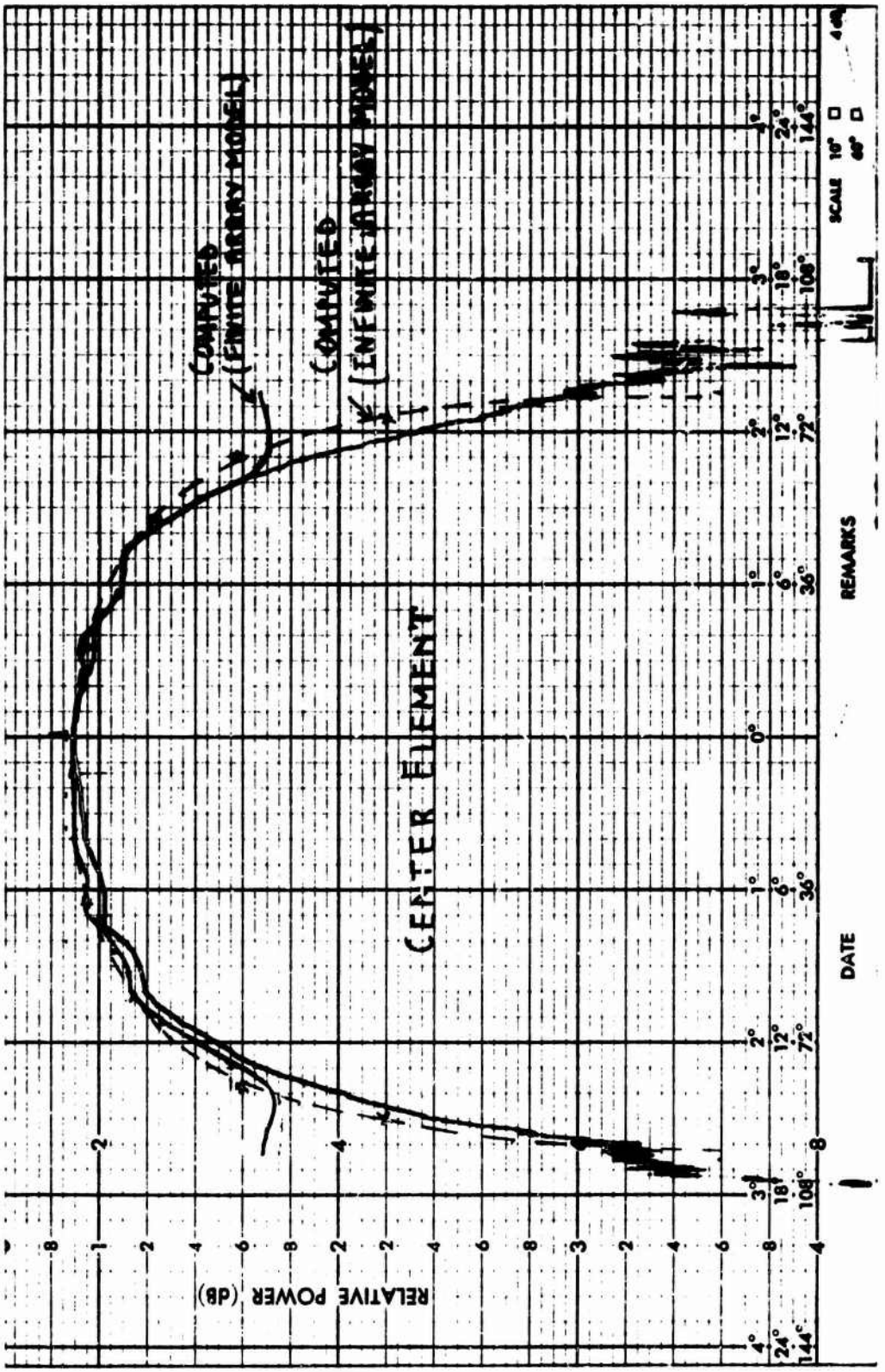

Figure 4-3 - Equiphase Match, Axial Polarization, Axial Cut

Figure 4-4 is the pattern in the axial plane of the edge element of the center column. The array is at the right of the radiator; polarization and matching conditions are as in the preceding case. The ground plane edge is very close to the element ($\approx 4\lambda$ away), so in the first 40 deg from endfire the left side of the experimental pattern is substantially different from the prediction based on infinite ground plane. On the side of the array the recorded data follow very closely the computed pattern up to about 12 deg from endfire. The measured (by the means of a horn standard) boresight gain of a center element is 5.4 dBi, which compares very well with the theoretical gain of 5.5 dBi, predicted by the infinite array model for an element matched in the boresight direction:

$$\text{Gain} = 4\pi \frac{A}{\lambda^2}$$

where A is the periodic cell area [14]. The measured boresight gain of the edge element is about the same as the gain of a center element. The boresight gain variation versus element position predicted by the finite array model is shown in Figure 4-5.

Figure 4-6 shows experimental and computed axial pattern cuts of an element at the center of the array, axially polarized, but with the matching arranged for the eigenexcitation $e(i/R = 0, w_o\ 2\pi/\lambda \sin 80°)$. The measured boresight gain of the element is 3.3 dBi, which compares very well with the theoretical gain of 3.5 dBi, predicted by both the finite and the infinite array model [1-2]. The element boresight gain variation versus position in the center column is shown in Figure 4-7. The elements are again matched for the eigenexcitation $e(i/R = 0, w_o = 2\pi/\lambda \sin 80°)$. For this matching condition Figure 4-8 gives computed and measured patterns of the edge element of the center column. The array is at the left of the excited radiator. By comparing Figure 4-8 with Figure 4-4 the effects of the different matching conditions can be clearly distinguished. The element pattern of Figure 4-4 is 11.5 dB below the boresight level at 75 deg from the element normal on the side of the array. The pattern of Figure 4-8 shows in the same direction a loss of only 6 dB. Analogous features are detected in Figure 4-3 is compared with Figure 4-6.

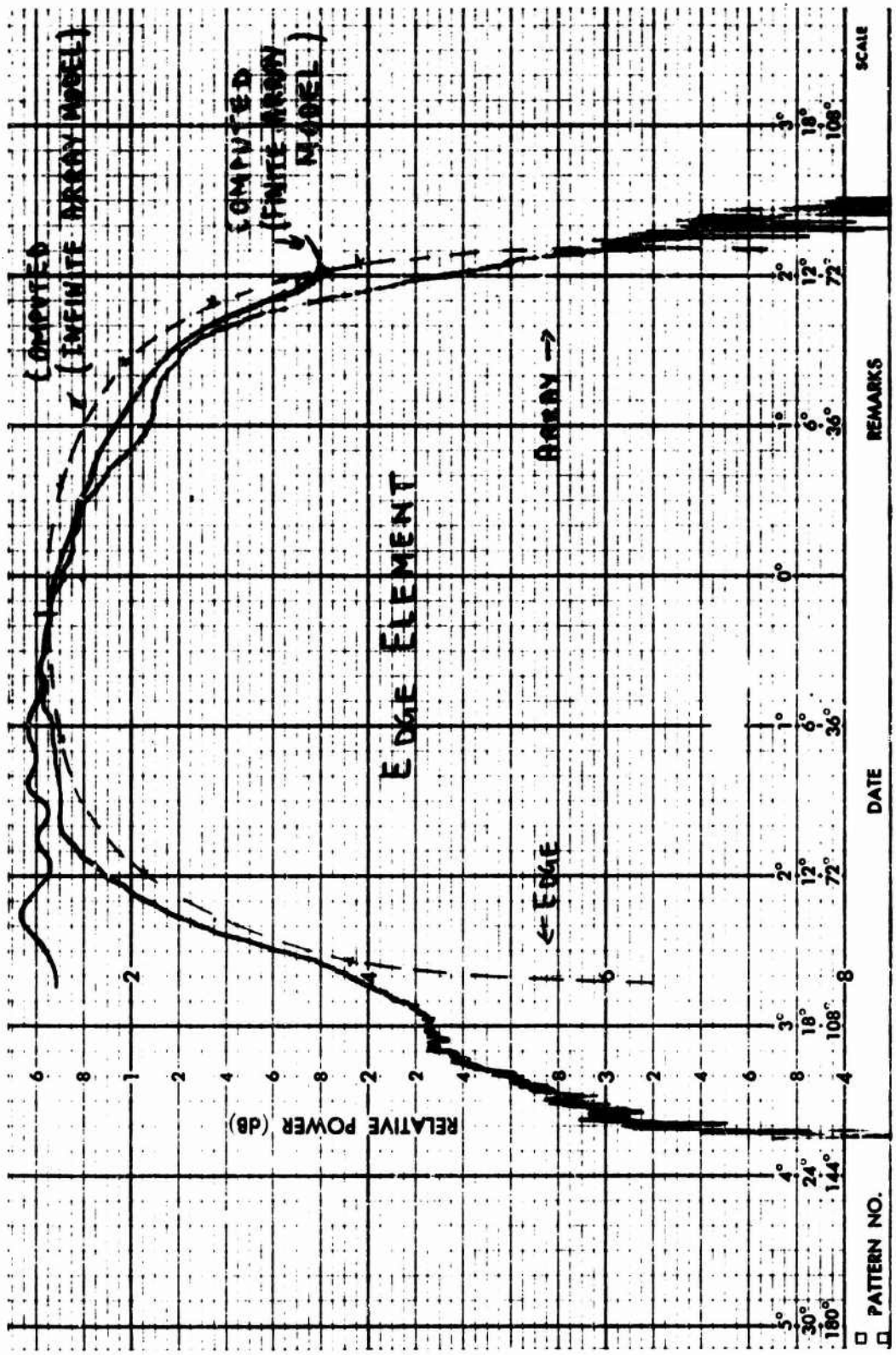

Figure 4-4 - Equiphase Match, Axial Polarization, Axial Cut

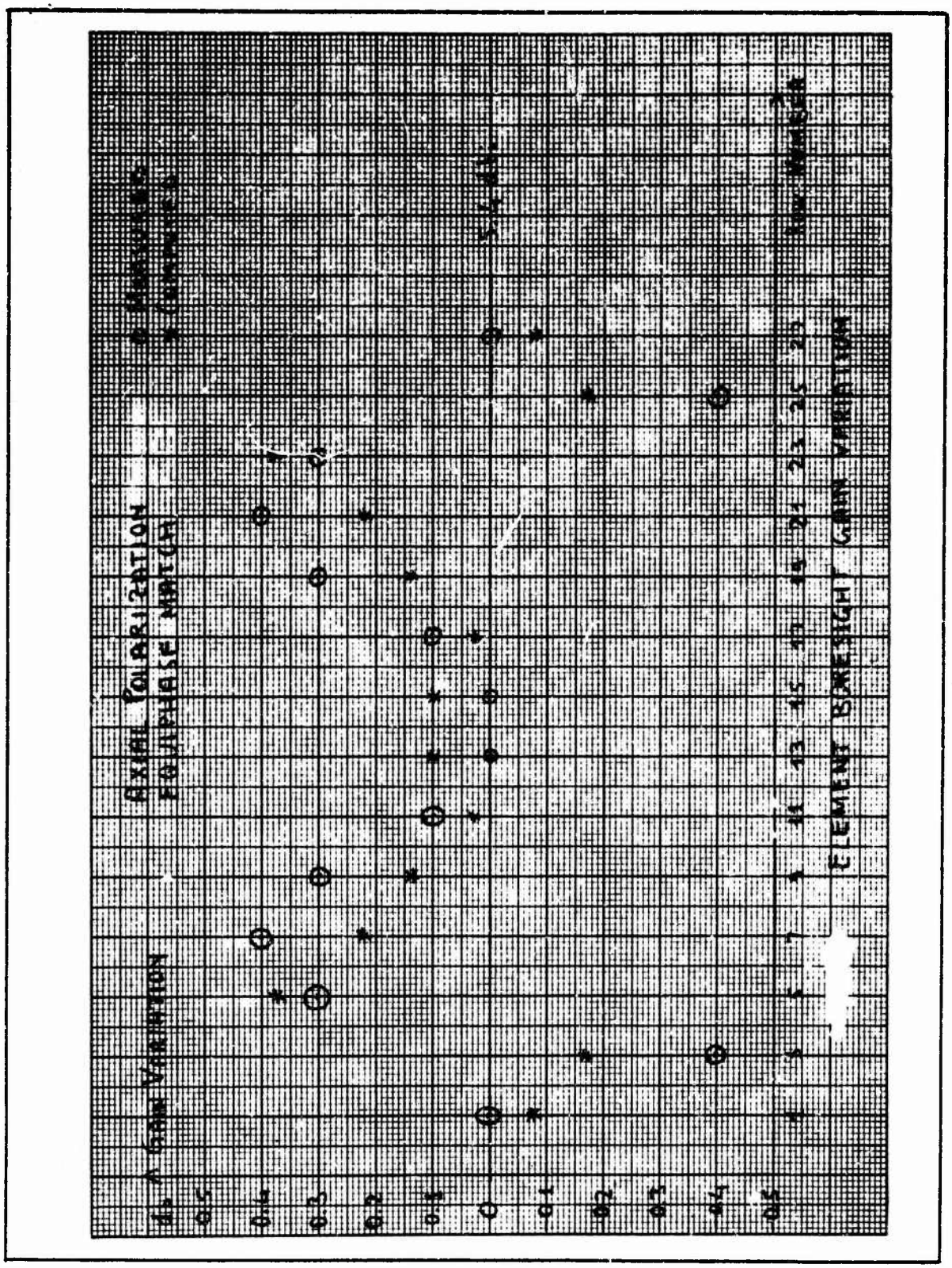

Figure 4-5 - Element Boresight Gain Variation

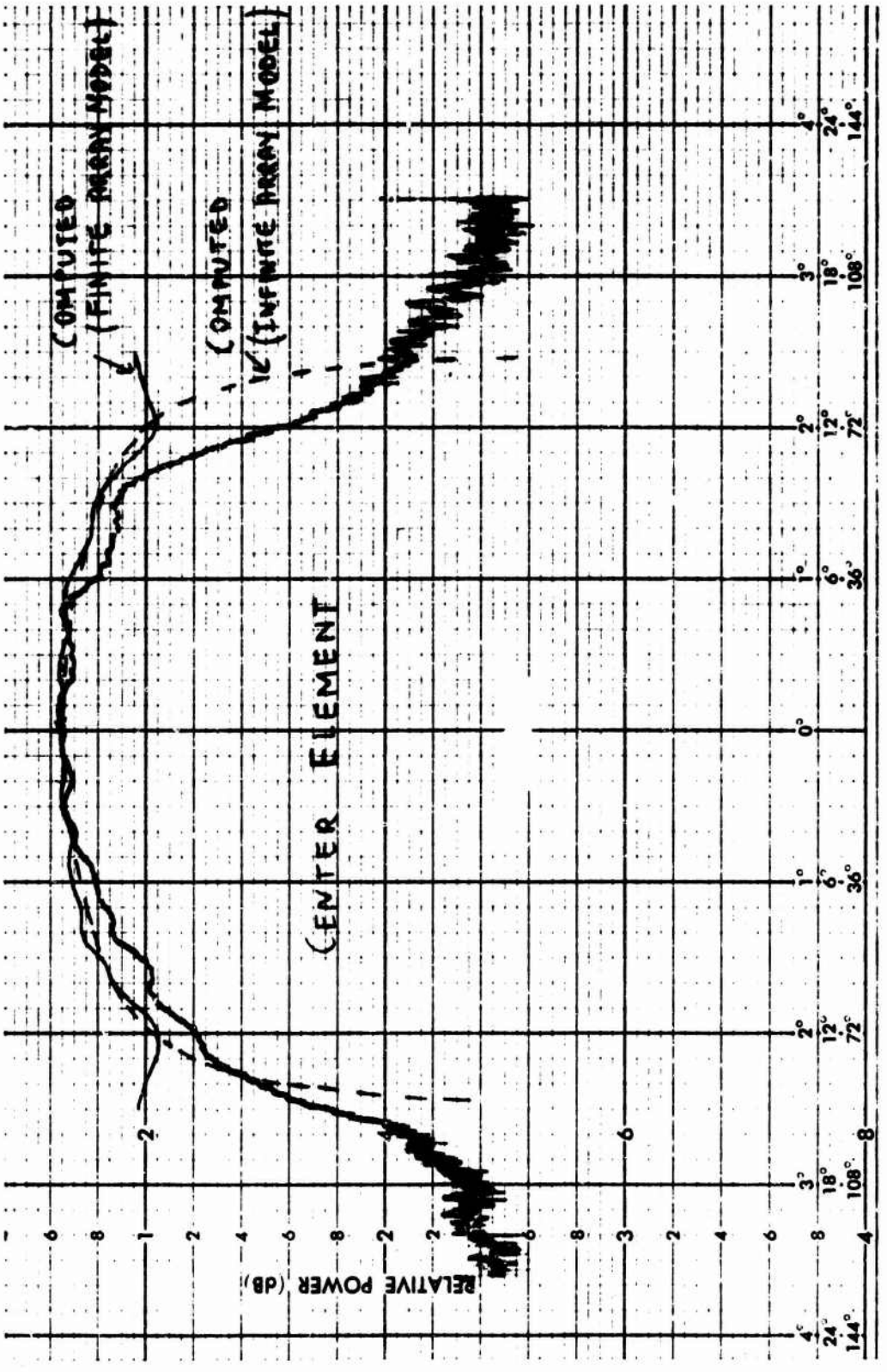

Figure 4-6 - Match for e(i/R = 0, w_o $2\pi/\lambda$ sin 80°) Axial Polarization, Axial Cut

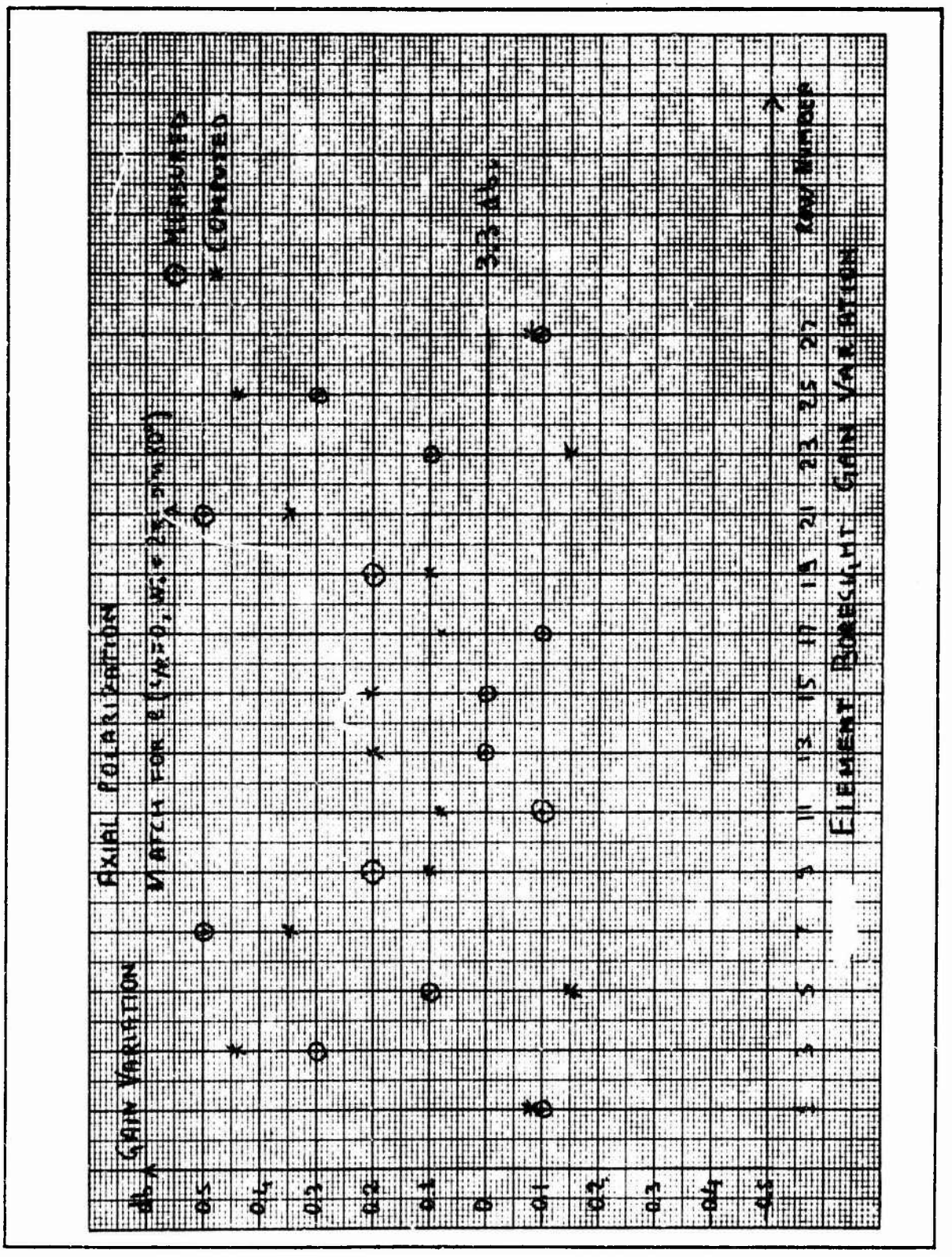

Figure 4-7 - Element Boresight Gain Variation

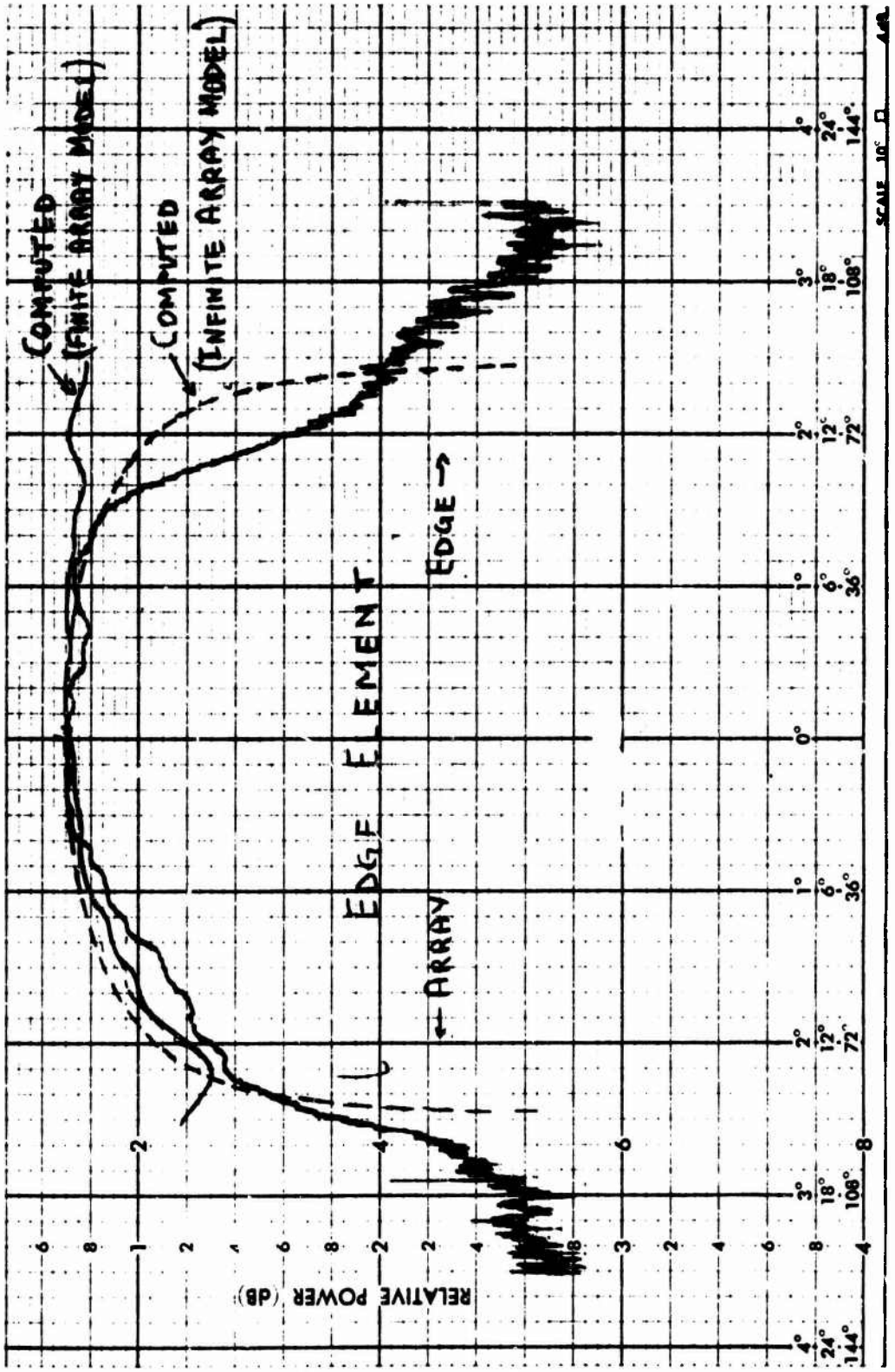

Figure 4-8 - Match for e(i/R = 0, $w_o = 2\pi/\lambda \sin 80°$), Axial Polarization, Axial Cut

Figure 4-9 shows the circumferential pattern of a center element axially polarized. The array is matched for the eigenexcitation e(i/R = 0, w_o = 0). Because of lack of edge effects, in the circumferential plane experimental and computed data are in excellent agreement down to very low level of radiation. The lack of edge effects from the array and from the ground plane, due to the polarization of the elements and the curvature of the cylinder, causes the element pattern to change very little as the element position is moved along the row (Figure 4-10). Analogous features are presented by the circumferential cuts of elements axially polarized and matched for e(i/R = 0, $w_o = 2\pi/\lambda \sin 80°$).

Excellent agreement between experimental and computed patterns is shown in the circumferential plane by circumferentially polarized radiators. Figure 4-11 gives the pattern of a center element. The array is matched for the eigenexcitation e(i/R = 0, w_o = 0). The infinite array model has been used in the computations. The element pattern does not change substantially going around a row in the circumferential sense as shown in Figure 4-12. The reason for this lies in the fact that the curvature has a bigger effect that the array edge. In order to have edge effects there must be a wave propagating along the array surface which is reflected at the edge and tends to alter the element excitation [2]. This is indeed what happens in the axial plane. In the circumferential plane this wave, instead of propagating along the array surface, tends to peel off the cylindrical surface and be radiated, so the edge is not strongly excited. These considerations are true for array sizes and cylinder radii around the value considered in this experimental program. If the cylinder radius is increased, and the array size is kept constant, one can expect the edge effects in the circumferential plane to become stronger.

Figure 4-13 shows the axial cut of an element at the center of the array. The polarization is circumferential and the match is for the eigenexcitation e(i/R = 0, w_o = 0). No relevant edge effects were detected for this pattern cut by moving the element to the border of the array (Figure 4-14). The pattern of a center element for circumferential polarization in the circumferential plane with the array matched for the eigenexcitation e(i/R = $2\pi/\lambda \sin 80°$, v_o = 0) is given in Figure 4-15. By comparing Figure 4-11 and Figure 4-15, one can see that the element pattern of Figure 4-15 is much

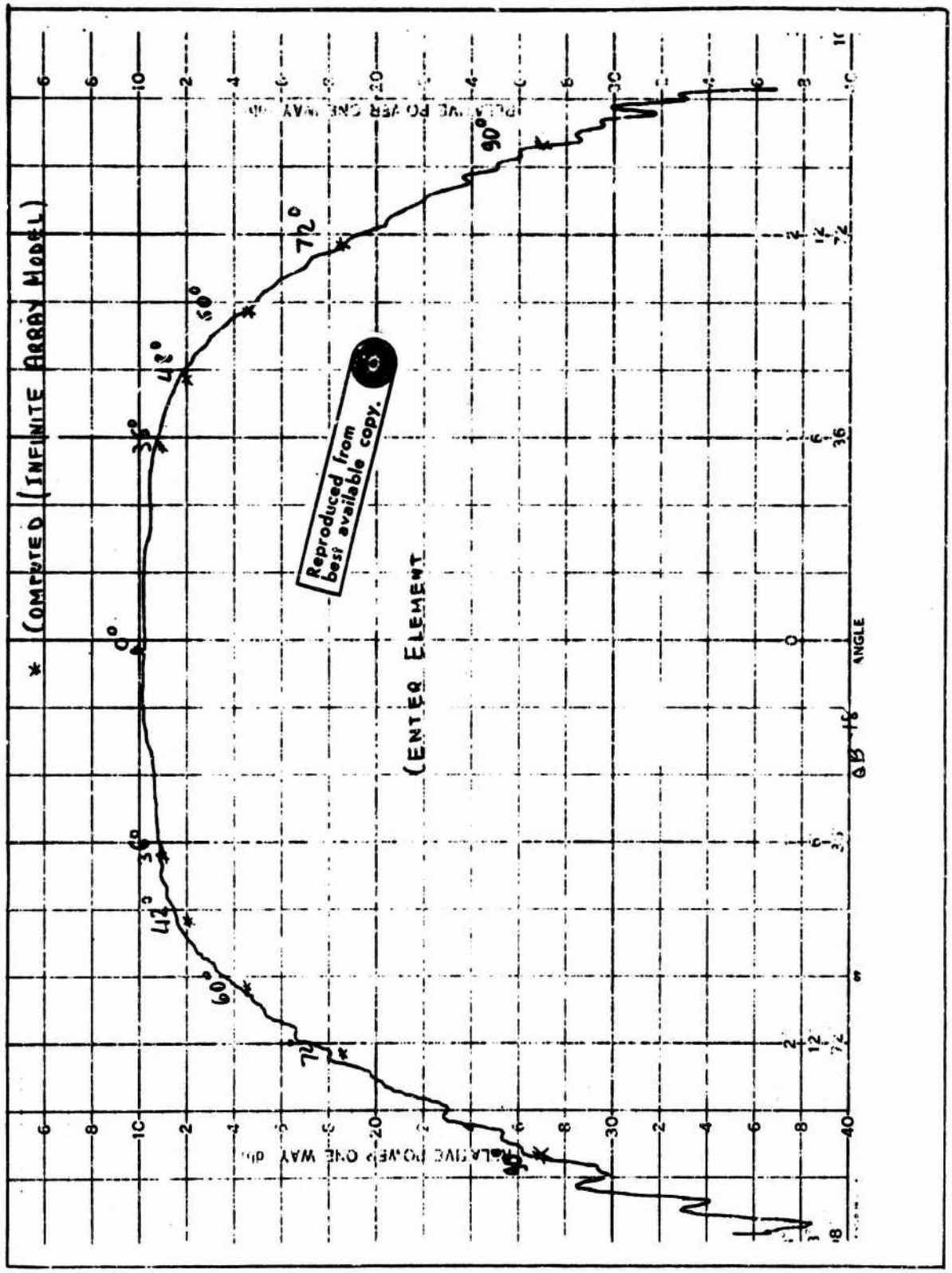

Figure 4-9 - Axial Polarization, Circumferential Cut, Equiphase Match

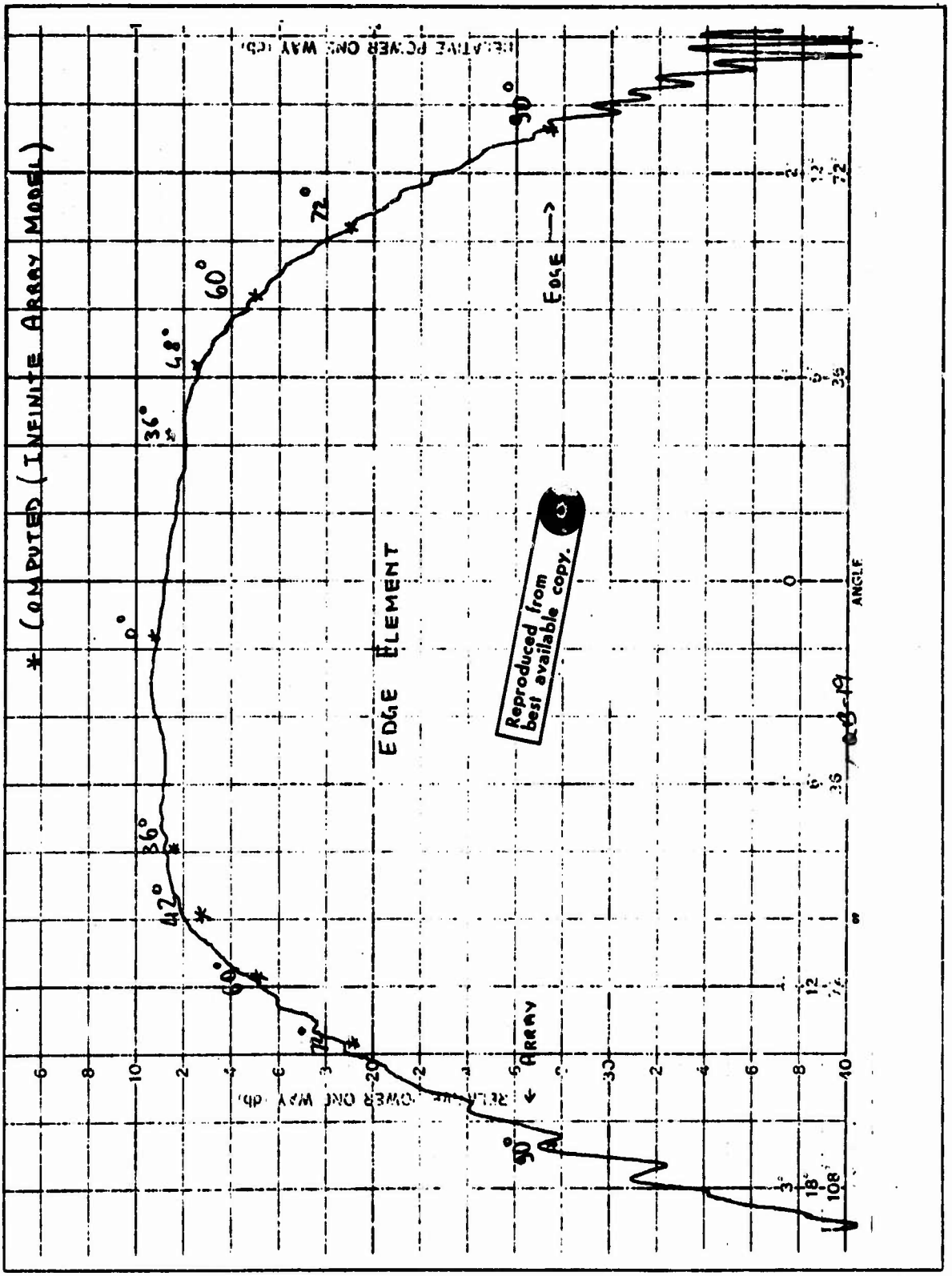

Figure 4-10 - Axial Polarization, Circumferential Cut, Equiphase Match

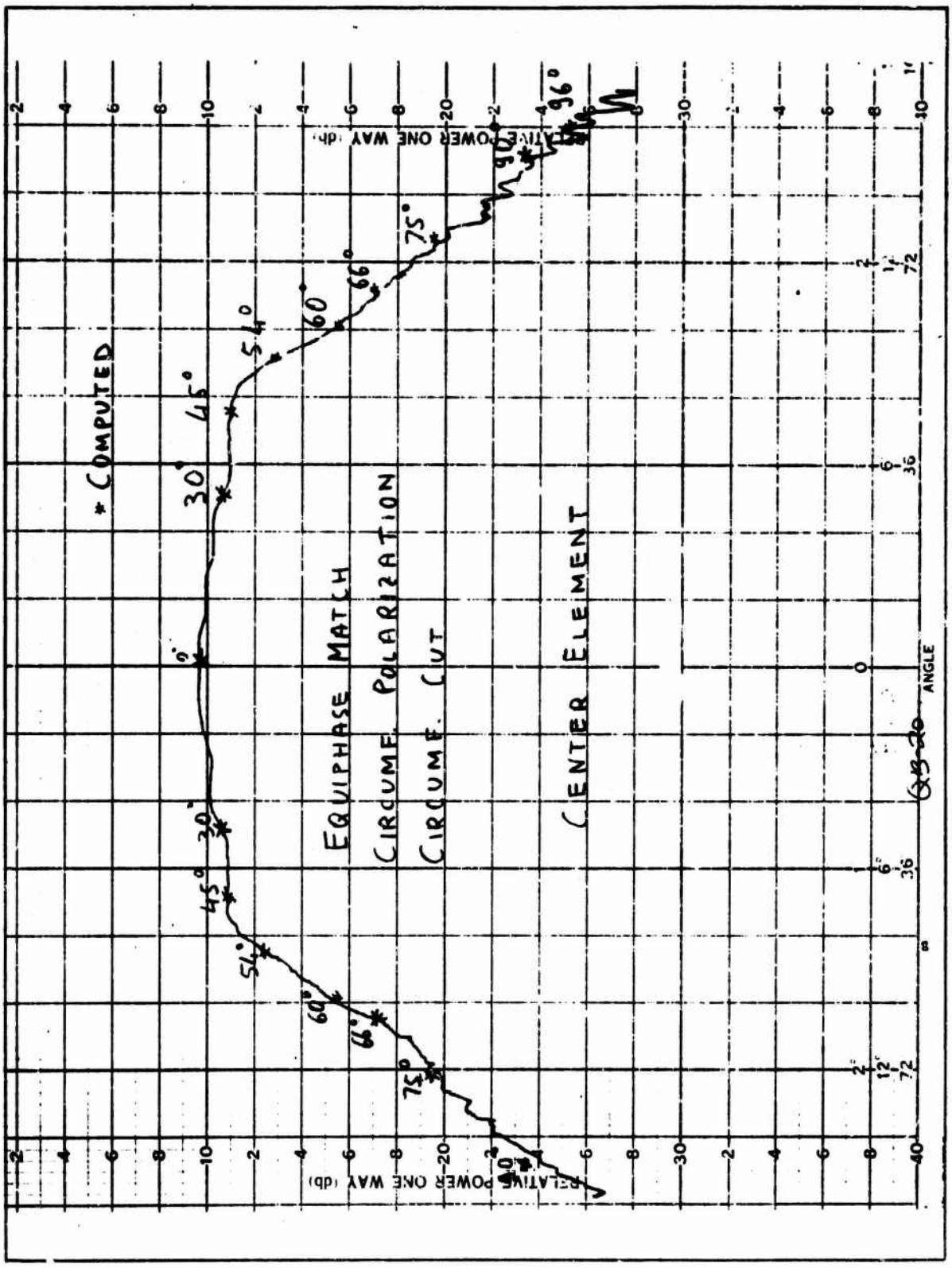

Figure 4-11 - Equiphase Match, Circumferential Polarization, Circumferential Cut

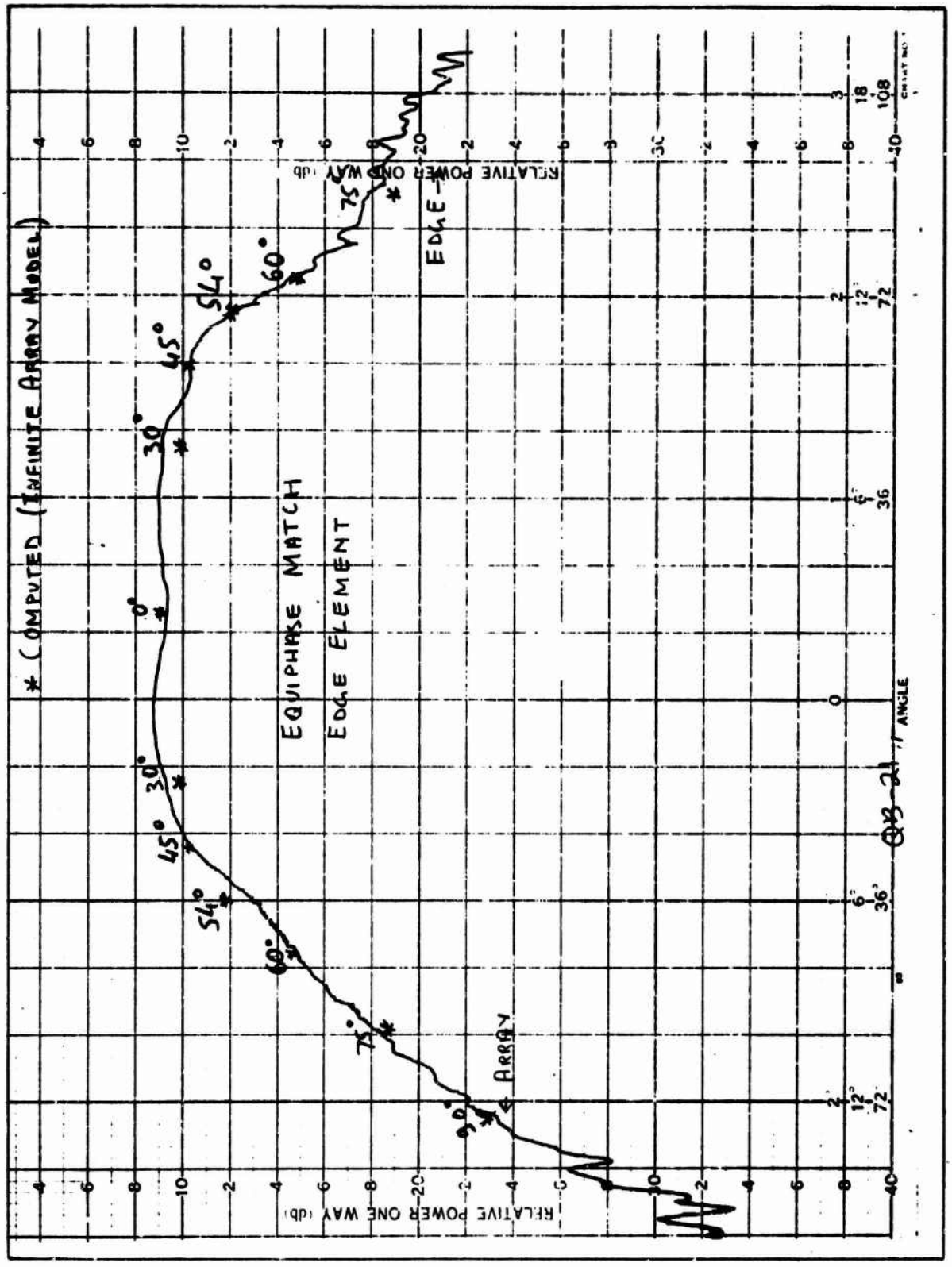

Figure 4-12 - Circumferential Polarization, Circumferential Cut

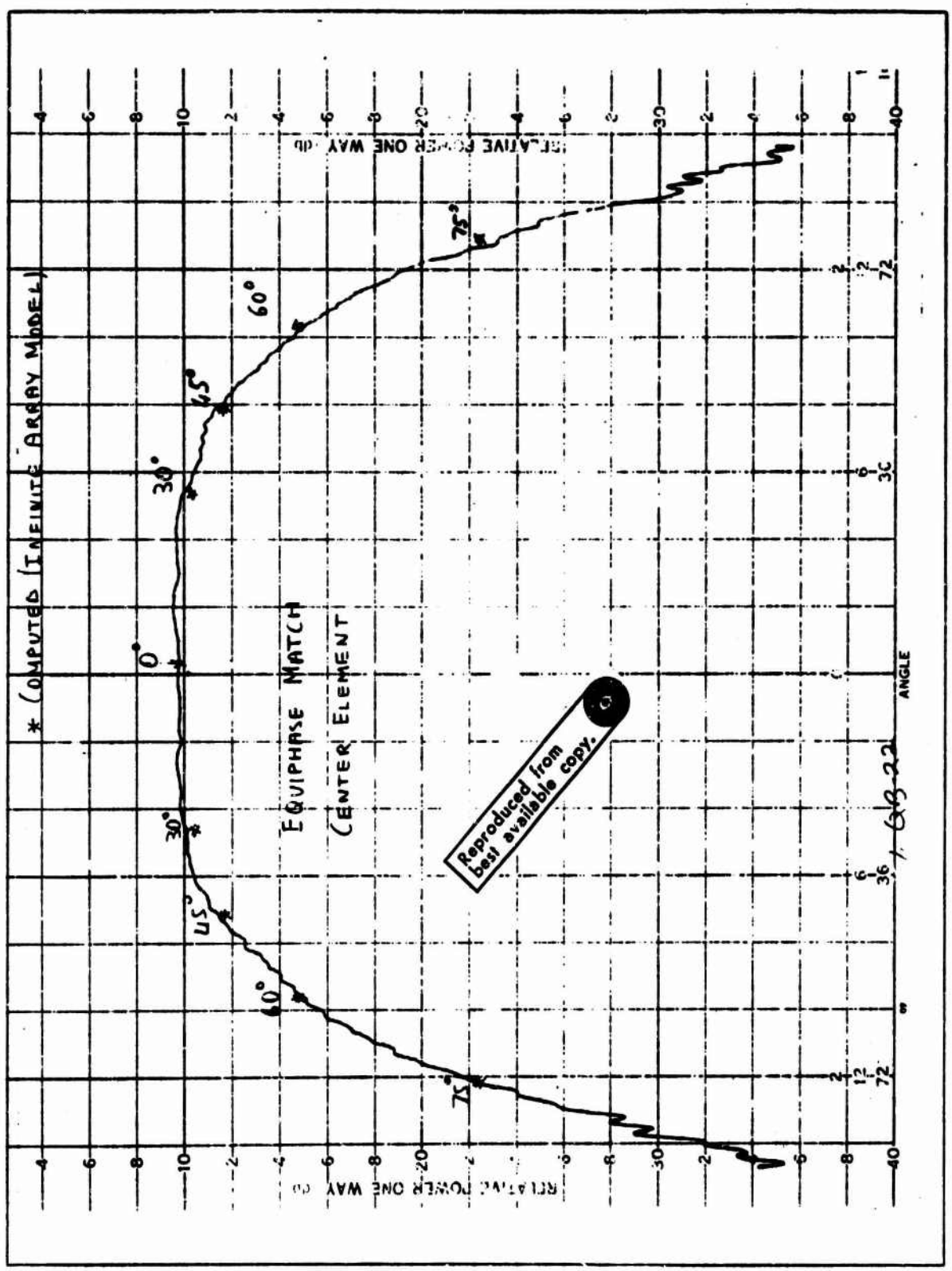

Figure 4-13 - Circumferential Polarization, Axial Cut

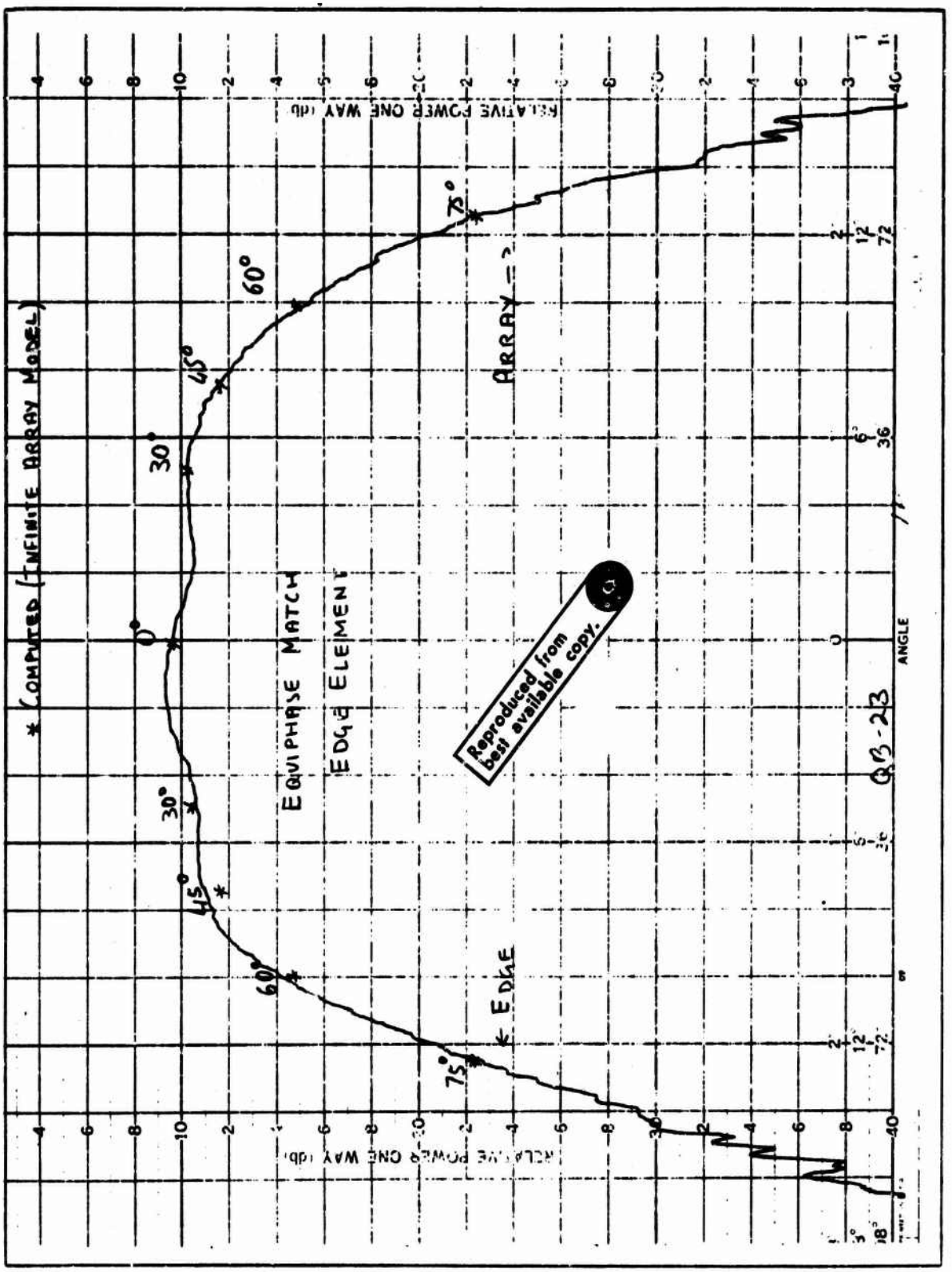

Figure 4-14 - Circumferential Polarization, Axial Cut

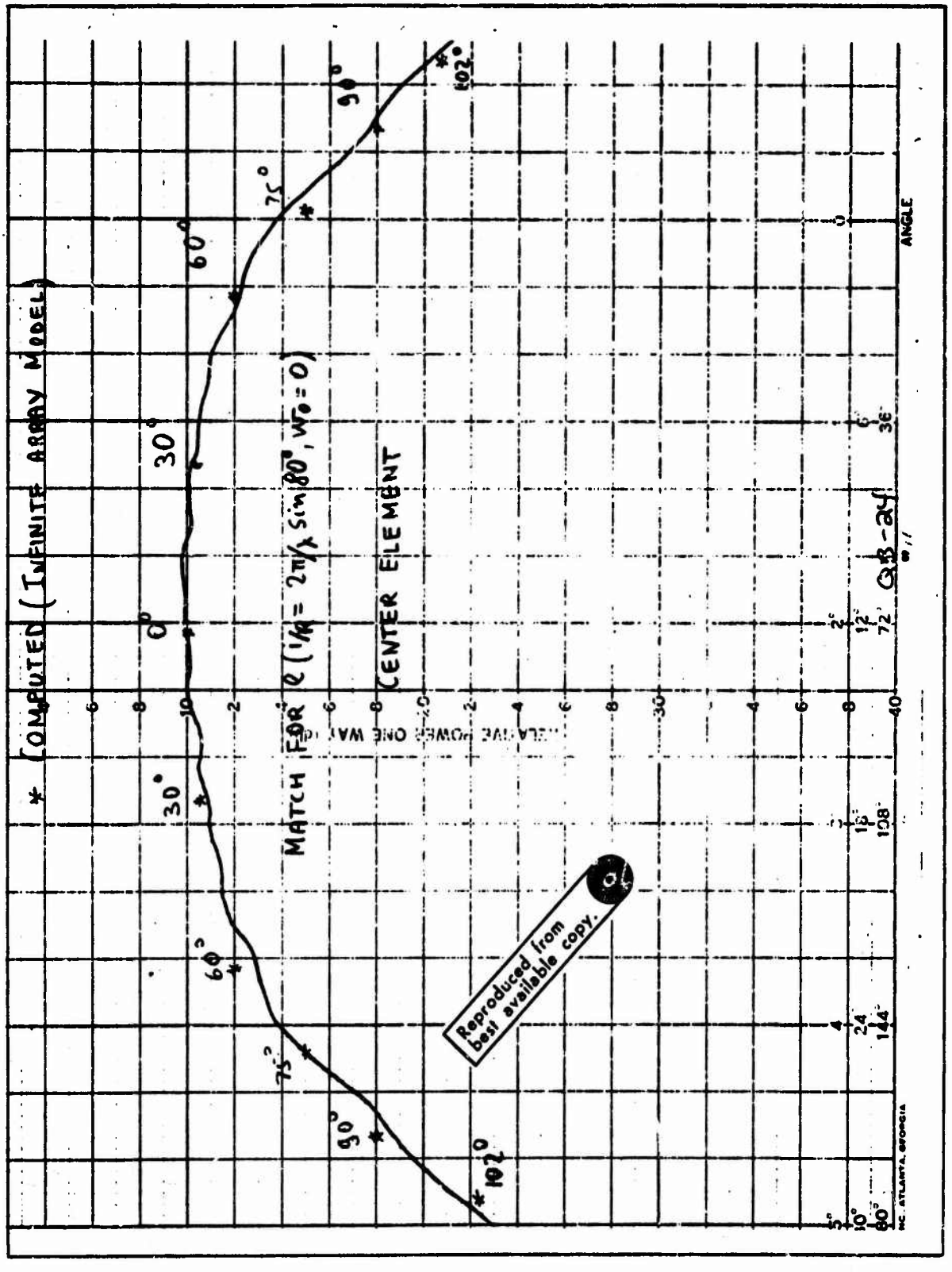

Figure 4-15 - Circumferential Polarization, Circumferential Cut

wider, an indication that a better array coverage has been achieved. The absolute boresight gain of the pattern of Figure 4-15 is 2.4 dBi, about 3 dB below the boresight gain of Figure 4-11. Both these values compare very well with the computations (2.3 dBi and 5.5 dBi, respectively).

As expected, edge effects are more pronounced for this matching condition than for equiphase match as seen in Figure 4-16. The element match tends to generate over the surface of the cylinder a wave, which, although partly radiated, excites the array edge more strongly than in the equiphase matching conditions.

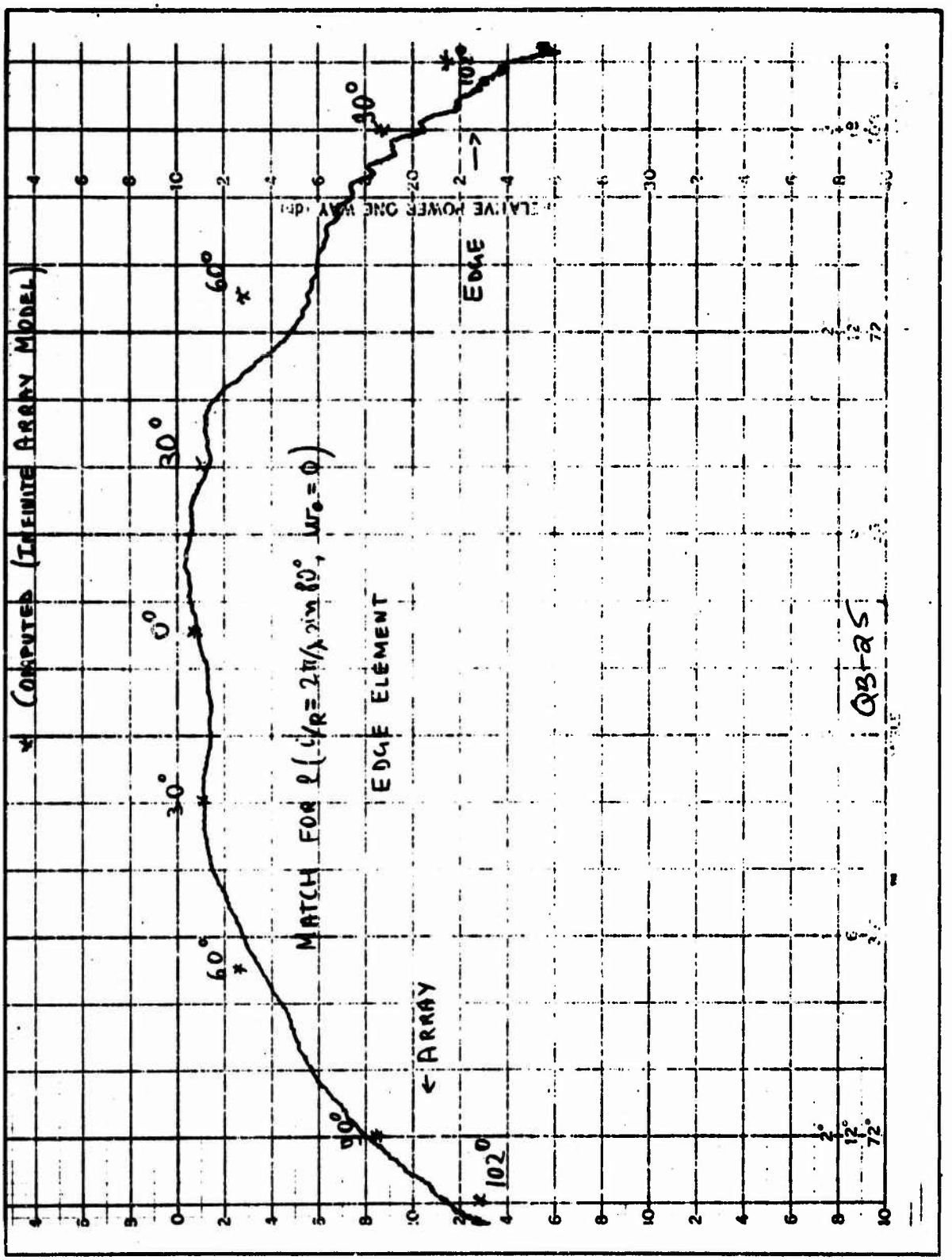

Figure 4-16 - Circumferential Polarization, Circumferential Cut

5. CONCLUSION

In this report some similarities between planar and conformal cylindrical arrays have been brought to light. The similarities have the important practical consequence of making the Wheeler simulator a design tool for cylindrical array elements in many instances.

The experimental program described in this report has proven that the theoretical methods developed previously and their coverage predictions [1-2] are indeed correct. The agreement between experimental and computed data has been consistently very satisfactory. In particular, the tests have shown that the realized gain element pattern can be modified by means of a microwave network inside the radiator waveguide [1]. The array pattern can be shaped so as to increase the scan coverage of the array.

In summary the multimode approach to the investigation of infinite cylindrical arrays and the experimental evidence of the correctness of this approach have brought cylindrical array theory to a state of refinement practically equal to that for the plane array.

APPENDIX A
FOURIER TRANSFORMS OF VECTOR MODE FUNCTIONS

Let us consider the wave number plane (u, w) and let us put:

$$t = \sqrt{u^2 + w^2} \quad ; \quad \cos \mu = \frac{u}{t} \; ; \quad \sin \mu = \frac{w}{t}$$

then the polar components of the Fourier Transform of the modes of a circular waveguide with radius "a" are given by [3] :

TE_{nm} modes:

$$\mathcal{E}_\rho = A n j^{n-1} \frac{\sin n\mu}{t} J_n(at) \tag{A1}$$

$$\mathcal{E}_\psi = A j^{n-1} \frac{a \cos n\mu}{1 - \left(\frac{at}{x'_{nm}}\right)^2} J'_n(at) \tag{A2}$$

For TM_{nm} modes:

$$\mathcal{E}_\rho = B j^{n+1} \sin n\mu \frac{t}{\left(\frac{x'_{nm}}{a}\right)^2 - t^2} J_n(at) \tag{A3}$$

$$\mathcal{E}_\psi = 0 \tag{A4}$$

where x'_{mn} and x_{nm} are the mode eigenvalues and J_n is a Bessel function and J'_n its derivative. The amplitude factors:

$$A = \frac{\sqrt{\frac{2}{\pi}}}{\sqrt{x'^2_{nm} - n^2}}$$

$$B = \sqrt{\frac{2}{\pi}}$$

are obtained by imposing the orthonormalization condition [3] :

$$\iint \underline{e}_i (\underline{s}) \; \underline{e}_k (s) = \delta_{ik} \qquad \text{(A5)}$$

The Fourier Transforms of the cross modes are obtained from Equations (A1) through (A4) by replacing μ with $\mu + \frac{\pi}{2n}$. From Equations (A1) through (A4), the rectangular components of the Fourier Transform of a mode are given by:

$$\mathcal{E}_u = \mathcal{E}_\rho \cos \mu - \mathcal{E}_\psi \sin \mu$$

$$\mathcal{E}_w = \mathcal{E}_\rho \sin \mu + \mathcal{E}_\psi \cos \mu$$

APPENDIX B
DERIVATION OF EQUATIONS (2-6) THROUGH (2-8)

Let us write Equation (5) as follows:

$$\underline{H}_t^+ (\underline{s}) = H_z (\underline{s})\, \hat{z} + H_\phi (\underline{s})\, \hat{\phi} \tag{B1}$$

Applying Galerkin's method, the difference between the expression (B1) and (2-4) for the magnetic field is $\underline{\rho}_o \times \underline{e}_a (\underline{s})$ scalarly multiplied by the magnetic vector mode function and integrated over the reference element aperture A. The following equation is obtained by using the orthonormalization condition Equation (A5):

$$[1 - \Gamma_a (\underline{u}_o)]\; G_{ao} + [1 + \Gamma_a (u_o)]\; jB_{ao} = \iint_A (e_{a\phi} H_z - e_{az} H_\phi) dA \tag{B2}$$

where $e_{a\phi}$ and e_{az} are the components of $\underline{e}_a (\underline{s})$.

In totally analogous manner, the following equations are obtained by projecting the difference between Equations (B1) and (B4) on $\underline{e}_c (s)$ and $\underline{e}_k (s)$.

$$-\Gamma_{ac} (\underline{u}_o) (G_{co} - j B_{co}) = \iint_A (e_{c\phi} H_z - e_{cz} H_\phi)\, dA \tag{B3}$$

$$-\Gamma_{ek}\, Y_k = \iint_A (e_{k\phi} H_z - e_{kz} H_\phi)\, dA \tag{B4}$$

By introducing Equations (B3) in (B5), the integrals in Equation (B2) through (B4) can be evaluated. Making use of the Fourier Transforms of the vector mode functions, the following expressions are established:

$$G_{ao}\ [1 - \Gamma_a\ (\underline{u}_o)] = [1 + \Gamma_a\ (\underline{u}_o)]\ [L_{aa}\ (\underline{u}_o) - jB_{ao}] + \Gamma_{ac}\ (\underline{u}_o)\ L_{ac}\ (\underline{u}_o) +$$

$$+\sum_{s=1}^{Q} \Gamma_{as}\ (\underline{u}_o)\ L_{as}\ (\underline{u}_o) \qquad \text{(B5)}$$

$$-G_{co}\ \Gamma_{ac}\ (\underline{u}_o) = [1 + \Gamma_a\ (\underline{u}_o)]\ L_{ac}\ (\underline{u}_o) + \Gamma_{ac}\ (\underline{u}_o)\ [L_{cc}\ (\underline{u}_o) - jB_{co}] +$$

$$+\sum_{s=1}^{Q} \Gamma_{as}\ (\underline{u}_o)\ L_{cs}\ (\underline{u}_o) \qquad \text{(B6)}$$

$$-\Gamma_{ak}\ (\underline{u}_o)\ Y_k = [1 + \Gamma_a\ (\underline{u}_o)]\ L_{ka}\ (\underline{u}_o) + \Gamma_{ac}\ (\underline{u}_o)\ L_{kc}\ (\underline{u}_o) +$$

$$+\sum_{s=1}^{Q} \Gamma_{as}\ (\underline{u}_o)\ L_{ks}\ (\underline{u}_o) \qquad \text{(B7)}$$

where the coefficients $L_{rt}\ (\underline{u}_o)$ (r, t = a, c, 1, 2...Q) are given by.

$$L_{rt}\ (\underline{u}_o) = \sum_{p=-\infty}^{+\infty} \sum_{q=-\infty}^{+\infty} [a\ (\underline{u}_{opq})\ \mathcal{E}^*_{ru}\ \mathcal{E}_{tu} + b\ (\underline{u}_{opq})\ \mathcal{E}^*_{ru}\ \mathcal{E}_{tw} +$$

$$-c\ (\underline{u}_{opq})\ \mathcal{E}^*_{rw}\ \mathcal{E}_{tu} - d\ (\underline{u}_{opq})\ \mathcal{E}_{rw}\ \mathcal{E}_{tw}] \qquad \text{(B8)}$$

where the star denotes complex conjugate. In Equation (B8) the simplified notations used mean that the functions in the square bracket must be calculated in the points of the lattice [1] of the u, w plane.

From Equations (B5) through (B7), Equations (B6) through (B8) are promptly established.

REFERENCES

1) Borgiotti, G. V., and Balzano, Q., "Analysis and Element Pattern Design of Periodic Arrays of Circular Apertures on Conducting Cylinders", Scientific Report No. 1, AFCRL-70-0682, November 1970, UNCLASSIFIED.

2) Borgiotti, G. V., and Balzano, Q., "End Fire Radiation from Planar and Large Cylindrical Arrays", Scientific Report No. 2, AFCRL-71-0322, May 1971, UNCLASSIFIED.

3) Borgiotti, G. V., "Modal Analysis of Periodic Planar Phased Arrays of Apertures", Proceedings of the IEEE, Volume 56, No. 11, November 1968, UNCLASSIFIED.

4) Borgiotti, G. V., and Balzano, Q., "Analysis of Periodic Phased Arrays of Circular Apertures". IEEE Trans. on Ant. and Prop. Volume AP-17, No. 2, March 1969, UNCLASSIFIED.

5) Amitay, N. and Galindo, V., "The Analysis of Circular Waveguide Phased Arrays", Bell System Tech. J. Volume 47, November 1968, UNCLASSIFIED.

6) Munger, A. D., et al, "Mutual Coupling on a Cylindrical Array of Waveguide Elements", IEEE Trans. on Ant. and Prop. Volume AP-19, January 1971, UNCLASSIFIED.

7) Sureau, J. C., "Realized Gain Pattern of Aperture Elements in Cylindrical Antenna Arrays", PhD Thesis, Politechnic Institute of Brooklyn, June 1971, UNCLASSIFIED.

8) Borgiotti, G. V. and Balzano, Q., "Analysis and Element Pattern Design of Periodic Arrays of Circular Apertures on Conducting Cylinders", Accepted for Publication on IEEE, Trans. on Ant. and Prop., UNCLASSIFIED.

9) Lee, S. W., et al, "Convergence of Numerical Solutions of Iris Type Discontinuity Problems", Hughes Aircraft Co., FR 70-14-594, August 1970, UNCLASSIFIED.

10) Diamond, B. L., "Small Arrays. Their Analysis and Their Use for the Design of Array Elements", Proceeding of the 1970 Phased Array Antenna Symposium, Polytechnic Institute of Brooklyn, June 2-5, 1970, Farmingdale, N. Y., UNCLASSIFIED.

11) Wheeler, H. A., "A Survey of Simulator Techniques for Designing a Radiating Element" Ibidem, UNCLASSIFIED.

12) Diamond, B. L., and Knittel, G. H., "A New Procedure for the Design of Waveguide Elements for a Phased Array", Ibidem, UNCLASSIFIED

REFERENCES (Cont.)

13) Borgiotti, G. V., "A Novel Expression for the Mutual Admimittance of Planar Radiating Elements", IEEE Trans. on Ant. and Prop., Volume AP-16, May 1968, UNCLASSIFIED.

14) Oliner, A. A. and Malech, R. G., "Pattern of an Element in a Passively Terminated Array Environment", Microwave Scanning Antennas, Volume 3, Hansen, R. C., Editor Academic Press, New York, 1966, pp. 301-308, UNCLASSIFIED.